The Economic and Environmental Cost of Pirate Avoidance

June 5, 2026

Renato Molina[1*], Juan Carlos Villaseñor-Derbez[2,3], Gavin McDonald[4,5,6], Grant McDermott[7]

[1]Department of Economics, Appalachian State University
[2]Department of Environmental Science and Policy, Rosenstiel School of Marine, Atmospheric, and Earth Science, University of Miami
[3]Frost Institute for Data Science and Computing, University of Miami
[4]Marine Science Institute, University of California, Santa Barbara
[5]Bren School of Environmental Science & Management, University of California, Santa Barbara
[6]Environmental Markets Lab, University of California, Santa Barbara
[7]Department of Economics, University of Oregon

*To whom correspondence should be addressed; E-mail: molinar@appstate.edu.

Abstract

Modern-day piracy remains a pervasive problem for the global maritime industry, yet its full economic costs and underlying mechanisms are largely unquantified. We explore this problem by pairing detailed pirate-encounter records with satellite tracking from more than 22 million shipping voyages between 2012 and 2023. Here, we show that vessels systematically reroute around recent encounters, with associated excess travel costs of over US$200 million per year and additional environmental damages of nearly US$582 million annually.

Introduction

Oceans have served as the main conduit of global trade for centuries. Today, maritime transport carries more than 70% of the world's traded goods by value and more than 80% by volume[1]. Yet the transportation of valuable goods has always created opportunities for predation. Maritime routes are particularly vulnerable because they are poorly enforced, and isolated vessels make ideal targets for ambush and escape. The complexity of multiple legal jurisdictions at play further complicates capture and prosecution. Thus, and despite its frequent historical associations, maritime piracy remains a significant problem today, with modern pirates still displaying organizational features documented for earlier eras[2–6].

Official records list more than 2,600 global pirate encounters between 2012 and 2023, with 166 taking place in 2023 alone (Fig. 1). Most of these encounters concentrate in busy trade channels, where pirates target high-value vessels for robbery or capture-to-ransom[7]. Fig. 1 **a** highlights three "hotspots"—the Gulf of Aden, the Gulf of Guinea, and the Malacca Strait in Southeast Asia—where pirate encounters have been particularly acute. The notable decline in encounters during 2018–2019 likely reflects sustained international naval operations, including the Combined Task Force 151[8] and the European Union Naval Force Operation ATALANTA[9], combined with the adoption of vessel-hardening Best Management Practices[10,11].

Despite the prevalence of maritime piracy, and compared to other trade frictions, there is relatively limited research on its welfare impacts. Previous efforts to quantify the cost of the problem suggest annual trade losses in excess of US$20 billion per year[12,13]. However, the mechanics underlying these costs are not clearly specified and estimates are often derived from aggregate trade (see Supplementary Note 1 for a detailed literature review and additional background on global piracy). A small number of micro-founded studies have begun to fill this gap[14,15], but to our knowledge none has used continuous, vessel-level tracking to observe how shippers adjust their behavior to piracy in real time.

In this work, we make two contributions. First, using a global grid dataset and analysis we identify and empirically measure the spatial avoidance of shipping behavior using a rich dataset that combines detailed voyage information with pirate encounters. Second, using a global voyage dataset and analysis we quantify the implied aggregate costs that can be attributed to piracy and the ripple effects on vessel behavior and global shipping. The datasets leveraged in these analyses include high-resolution spatio-temporal information on pirate encounters from the US National Geospatial Intelligence Agency Anti-Shipping Activity Messages (ASAM) database[16], as well as individual vessel tracks of all known cargo, tanker, and refrigerated vessels that use the Automatic Identification System (AIS) globally[17]. Our empirical results show that a pirate encounter diverts maritime traffic away from the area for about 6 to 7 days. These

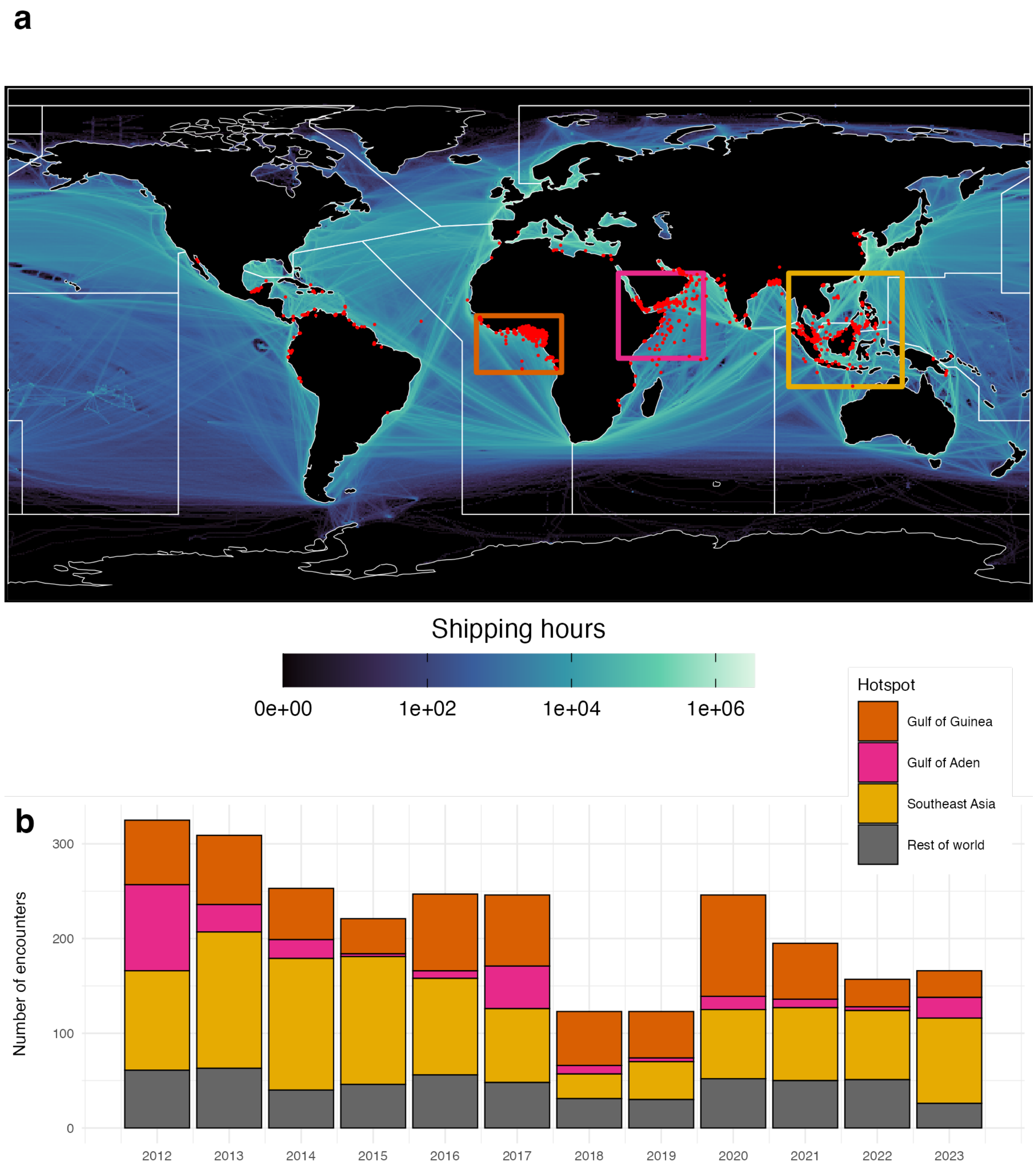

Figure 1: **A global view of modern-day maritime transport and piracy.** **a** shows the spatial overlap of shipping activity and pirate encounters from 2012 to 2023. Note that data are $\log_{10}$-transformed for visualization purposes and represented using a $0.5° \times 0.5°$ grid in geographic coordinates, with the fill color of each pixel representing the total shipping transit time from 2012-2023 (hr). Pirate encounters are shown as red points. The colored overlay bounding rectangles correspond to the three main piracy hotspots, namely: 1) Gulf of Guinea, 2) Gulf of Aden, and 3) Southeast Asia. The bounding boxes for hotspots are defined by a density-based clustering approach (see Methods). Outlines of the major Anti-shipping Activity Messages (ASAM) regions are shown as white lines. **b** shows the number of pirate encounters across hotspots and the rest of the world from 2012 to 2023.

adjustments, along a shipping route, can be associated with a marginal increase of about 54 ($\pm$ 8.7; M $\pm$ CI) kilometers or 3 ($\pm$ 0.5) hours per voyage per additional past encounter. When aggregated at the global level, and taking into account prevailing fuel and labor costs, these adjustments suggest additional transportation costs of US$365 million during 2023 (annual average 2012-2023 of US$209 million). Moreover, we estimate that surplus emissions of air pollutants (CO_2, NO_x, and SO_x) due to increased fuel usage yield an annual average of US$582 million in environmental damages. About 22% of NO_x and SO_x emissions take place in coastal waters, which is where they cause the most damage.

Results

A case study in piracy avoidance

To avoid ambiguity, it will prove helpful to define precisely several terms that we use in our analysis. A *route* is a port-to-port combination, a *voyage* is a trip made along a route, and a *path* is the sequence of coordinates chosen by the vessel to travel a route. With these definitions in hand, let us consider a case study of how individual vessels might respond to the threat of piracy. Specifically, how should shippers respond to information about pirate presence along their route? We can reasonably assume that total deterrence and enforcement options are too costly and logistically cumbersome for most individual vessels to bear. As such, short-term adaptation in the form of avoidance and/or vessel protection provide the best courses of action. Only the first of these can be systematically observed for the entire industry, and therefore avoidance behavior is the subject of our analysis.

Fig. 2 depicts the behavioral response to a 2013 pirate encounter in the Makassar Strait near Indonesia. On June 19, the anchored Hong Kong-flagged bulk carrier OCEAN GARNET was boarded at the Muara Jawa Anchorage by three to five armed robbers, who fled when the deck watch raised the alarm; the incident was immediately broadcast to other vessels in the region via the ASAM communication network, a global service provided by the United States Office of Naval Intelligence[18]. This information allowed vessels in the area to rapidly adjust their behavior; we observe a near-total avoidance of the encounter area following the ASAM broadcast. The previous cluster of shipping activity near the Muara Jawa Anchorage—marked by an orange "X" on the map—all but disappears (Fig. 2 **a**). The number of voyages in the affected area also drops from an average of 21 per day to just 3 per day (Fig. 2 **a**).

Quantifying global avoidance behavior

Fig. 2 provides evidence of avoidance behavior following a single piracy event. In this section, we expand our analysis to the global level and quantify the extent to which shippers take adaptive measures to avoid areas of active pirate risk. Formally, we test whether vessel operators modify their behavior after a piracy encounter becomes public knowledge using two distinct empirical approaches.

First, we examine adaptation over geographic space, where $0.5° \times 0.5°$ grid cells are the unit of observation. Following the Makassar Strait example, our goal is to establish patterns of vessel avoidance, consistent with a behavioral adjustment that yields fewer transits through a region after an attack. We evaluate this prediction formally by testing for systematic changes in daily transit activity within all $0.5° \times 0.5°$ grid cells that experienced reported pirate activity between 2012 and 2023 (N = 618 grid cells and 1,960 pirate events). The results are summarized as a series of event study plots in Fig. 3 and reveal a clear pattern of geographic redistribution in grid-level vessel activity following a pirate event. Specifically, we estimate that a piracy event causes a 7-9% drop in average occupancy time (Fig. 3a) and a 15-19% drop in total distance traveled (Fig. 3b) within an affected cell during the subsequent week. Fig. 3e–f show that this effect is mostly driven by a reduction in the number of vessels and trips transiting through a grid cell, rather than by behavioral adjustments within a grid cell (e.g., vessels taking shorter paths within a cell).

Our spatial results are robust to a variety of specification tests and modeling choices, including different transit measures, changes in grid resolution, and estimator features (e.g.,[19]). Similarly, we demonstrate robustness against behavioral confounders such as the potential for shippers to intentionally disable their AIS transponders; an emergency safety measure officially allowed by the International Maritime Organization if a captain fears their ship is in danger of piracy[20]. See Supplementary Note 5 for more information about these robustness checks.

Having established that vessels reroute in response to encounters (spatial adjustment), we now consider the operational costs of navigating piracy-active corridors. Our second empirical

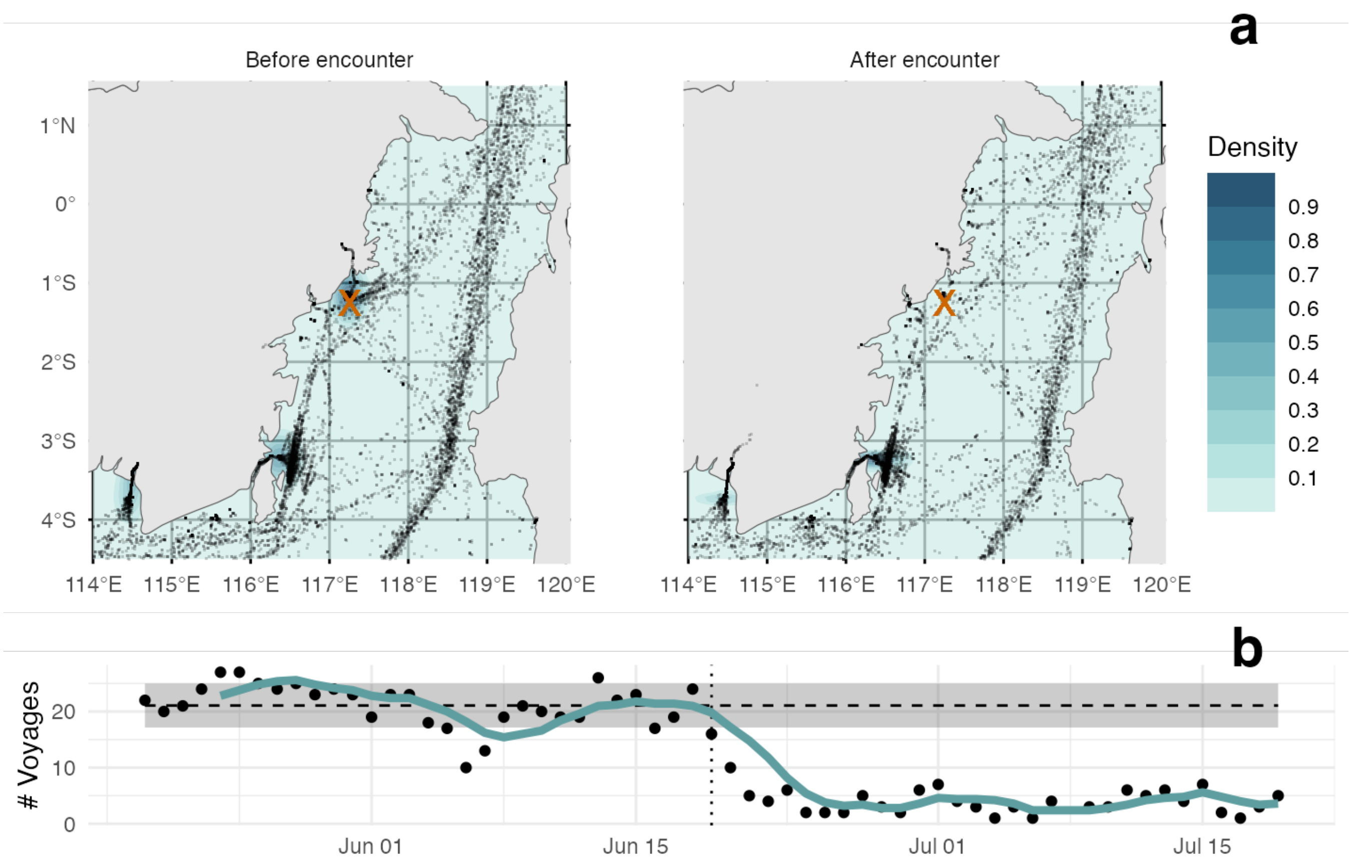

Figure 2: **"X marks the spot": Example of change in shipping vessel transit following an encounter with pirates on June 19, 2013 off the coast of Indonesia. a** shows maps of the Muara Jawa Anchorage one week before (left) and after (right) the pirate encounter. Black points show vessel positions, and background colors show a 2-dimensional kernel estimate of vessel density. **b** shows a time series of daily number of voyages crossing the affected pixel (at 117E, 1.5S, indicated with an orange "X"). Each point shows the total daily number of voyages, and the solid line shows the mean number in a 5-day rolling window. The horizontal dashed line and shaded area show the baseline number of daily voyages (mean ± standard-deviation) before the attack.

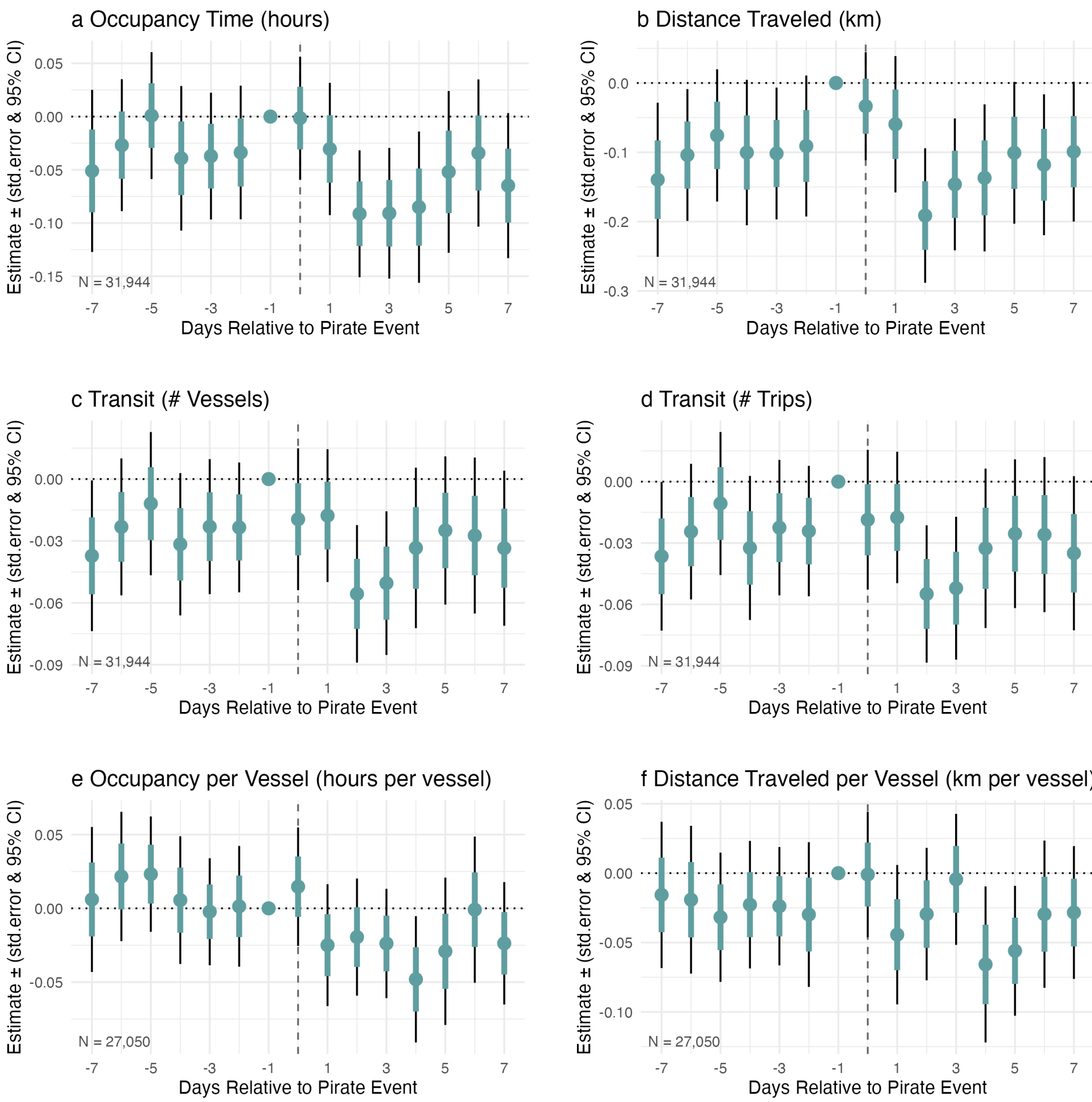

Figure 3: **Dynamic effects of piracy on ship transit.** The unit of observation is a grid cell-day. Each inset examines a different shipping activity measure. The horizontal axis shows time (days) relative to the timing of a pirate event. The vertical axis shows the magnitude of the effect. Points are coefficient estimates from Equation (1), showing the change in shipping activity relative to one day before the attack ($k = -1$). Inset numbers in the bottom-left corner are sample sizes after accounting for singletons and unavailable outcome variables (e.g., hours / vessel when # vessels = 0). All models include grid-cell-by-month and date fixed effects. The thick portion of error bars shows Conley standard errors (50 km cutoff), and the thin portion shows 95% Confidence Intervals.

approach therefore reframes the problem in terms of individual vessel voyages, i.e., where *voyage* is the unit of observation. The regression results are summarized in Table 1, with additional details in Supplementary Note 2. We observe that a piracy encounter along a vessel's likely voyage path is associated with longer average travel distances and prolonged travel times. The global estimate suggests that an additional pirate encounter—within the preceding 7 days and along a vessel's likely voyage path—translates to an extra 54.3 km in distance and 2.8 hr in travel time. We observe consistent results when restricting the sample to voyages that traverse hotspots, although the effect is much more pronounced for voyages passing through the Gulf of Aden (245.7 km and 9.8 hr, respectively). Supplementary Note 4 extends this analysis and shows that these additional distances are not driven by vessels abandoning their routes or switching to entirely different maritime corridors within a route.

In contrast to the economically meaningful impacts on travel distance and time, the effect on speed is still positive but minimal. We interpret these results as an indication that adjustments to speed are less cost-effective as an avoidance measure, or technically infeasible due to engine and vessel constraints. We also note that this behavior is consistent with optimal avoidance, since the cost of each additional unit of distance traveled grows linearly, while the cost per each additional unit of cruising speed grows approximately exponentially[21]. These results are robust to specification, subsampling, and data construction decisions. Supplementary Note 5 provides details and robustness tests.

The costs of piracy

How much does all of this avoidance behavior cost in monetary terms? While operational costs are not directly observable to us, we can address this question by using vessel characteristics to determine the likely fuel and labor requirements along a given voyage. The results from this exercise are available in Supplementary Note 2. Summarizing, and consistent with our other findings, we estimate that one additional pirate encounter during the preceding 7 days is associated with an average increase of about US$2,300 in input costs per voyage (comprising about US$1,900 in fuel and US$400 in labor). While this effect remains largely consistent across data samples, again we observe a considerably larger effect in the Gulf of Aden. Our estimates for this hotspot suggest that an additional pirate encounter is associated with a

Table 1: Effect of Past Pirate Encounters on Shipping Voyages.

	Global	G. of Aden	G. of Guinea	S.E. Asia
Panel (A): Total Distance (km)				
Encounters (7 day)	54.28***	245.69***	46.32***	37.29***
	(4.45)	(31.35)	(3.83)	(4.01)
Panel (B): Total Time (hr)				
Encounters (7 day)	2.82***	9.78***	3.07***	2.00***
	(0.24)	(1.28)	(0.30)	(0.24)
Panel (C): Average Speed (km h^{-1})				
Encounters (7 day)	0.04***	0.32***	0.06**	0.03***
	(0.01)	(0.05)	(0.03)	(0.01)
Observations	22,896,864	888,075	316,716	4,560,514
Hotspot FE	X	•	•	•

* $p < 0.1$, ** $p < 0.05$, *** $p < 0.01$ The unit of observation is a voyage. Estimates are from Equation (2). Each panel examines an observed feature in terms of total distance in kilometers (km), total time of the voyage in hours (hr), and the average speed of the voyage (km h^{-1}). Each column is a different sample: Global uses the full sample; G. of Aden, G. of Guinea, and S.E. Asia restrict to voyages passing through each hotspot, respectively. Encounters (7 day) is the count of pirate encounters recorded in the projected path of the vessel in the preceding 7 days from the departure date using a 5-degree spatial footprint. The sample spans from 2012 to 2023. Controls include average wind speed, the wind-resistance index, and average wave height along the voyage. Fixed effects include country-to-country combination, vessel type, vessel size, hotspot, top route, and month-by-year. X indicates the fixed effect is included; • indicates the fixed effect is absorbed by the sample restriction. Standard errors are clustered by country-to-country route by year.

per-voyage cost of roughly US$10,600 (US$9,400 in fuel plus US$1,200 in labor).

Increases in fuel consumption, however, have an additional environmental and social impact due to the emissions of greenhouse gases and local pollutants that are harmful to human health. Implementing a similar approach as with fuel and labor, here we focus on CO_2, NO_x and SO_x emissions, since these pollutants are particularly relevant for the shipping industry[22,23]. Detailed results by year and pollutant are provided in Supplementary Note 2. Overall, we estimate that an additional pirate encounter in the preceding 7 days is associated with an approximate increase of 8 tons of CO_2, 200 kg of NO_x, and 165 kg of SO_x per voyage, respectively. NO_x and SO_x excess emissions are relatively less voluminous, but this is to be expected given their smaller concentrations in bunker fuel relative to carbon[24]. Once again, limiting the analysis to the Gulf of Aden suggests impacts that are an order of magnitude larger.

To contextualize the practical significance of these estimates, we contrast the implied operational and pollution costs of avoidance behavior during our full 2012–2023 sample with a counterfactual scenario that is absent any pirate activity. Fig. 4 **a-d** maps the average annual costs to the shipping industry (fuel and labor costs), and the additional emission of air pollutants. To monetize impacts, we use a conservative estimate of the social cost of each pollutant[25,26] and derive an aggregate measure of the global costs of piracy that averages to US$791 million per year. Approximately US$209 million of this topline number are attributable to private operational (fuel and labor) costs, while US$582 million are attributable to public damages (due to climate change and air pollution). ASAM regions 7 and 9 (containing the Southeast Asian hotspot) account for US$378 million and US$143 million, ASAM region 6 (containing the Gulf of Aden) accounts for US$135 million, and ASAM region 5 (Gulf of Guinea) accounts for US$84 million (Fig. 4**e**).

The results underlying Fig. 4 are reported in detail in Supplementary Note 3. We note that NO_x and SO_x are pollutants that mostly affect the region where they are emitted. We can constrain the impacts of NO_x and SO_x emissions to each nation's Exclusive Economic Zone (200 nautical miles) or Territorial Seas (12 nautical miles). In doing so, we find that US$469 million (86.09%) of the total costs from these two pollutants occur within Exclusive Economic Zones, and that US$124 million (22.82%) occur within the Territorial Seas.

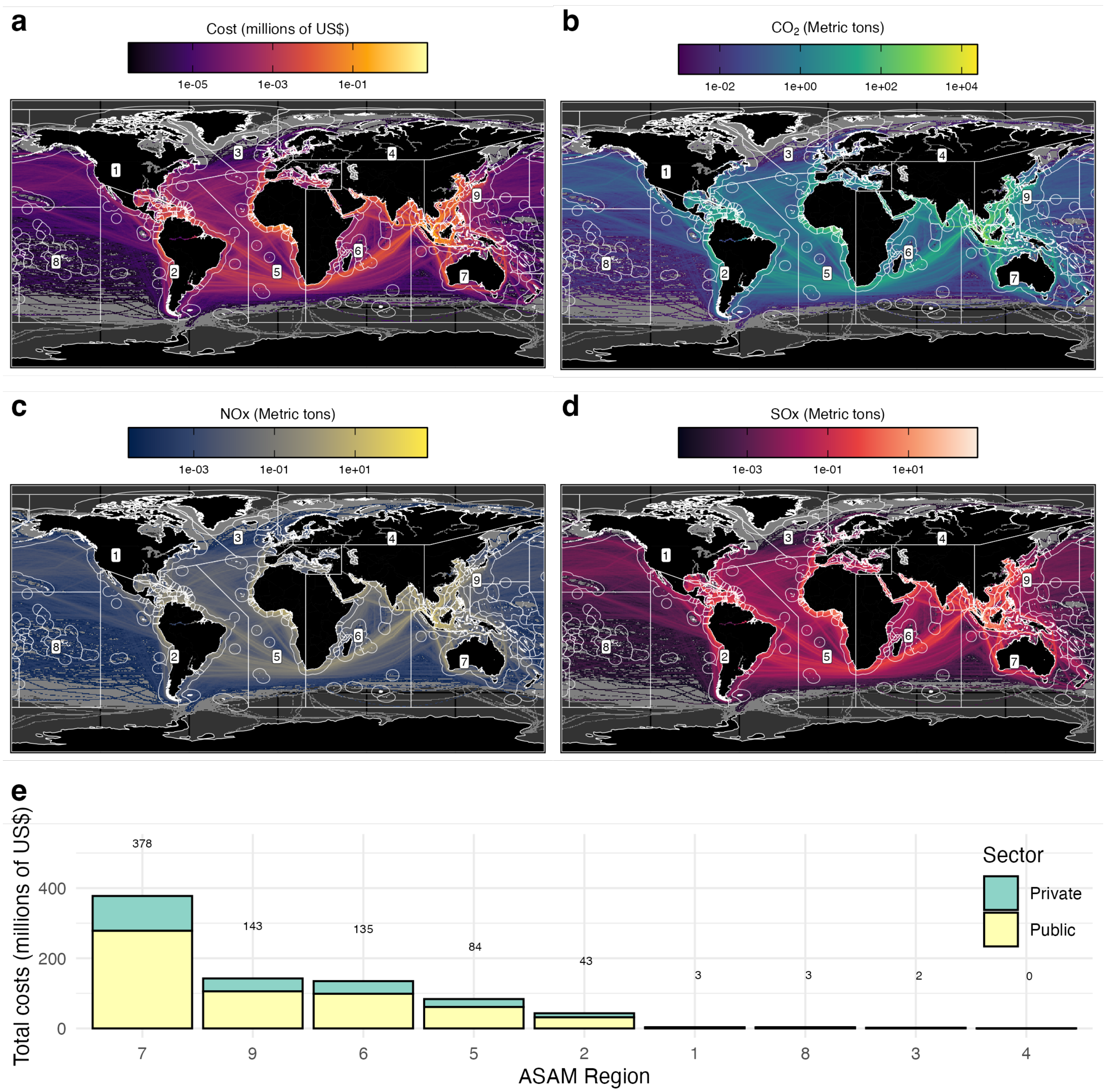

Figure 4: **Additional Operational Costs and Emissions due to Piracy. a** maps the mean annual private costs to shippers (labor and fuel costs; Million USD). **b-d** map additional CO_2, NO_x, and SO_x emissions (Metric tons). Note that data are $\log_{10}$-transformed for visualization purposes and represented using a $0.5° \times 0.5°$ grid in geographic coordinates. **e** shows the total costs (Million USD) associated with piracy by ASAM region, where we sum private costs to shippers as well as the cost of damages imposed by additional emissions based on the social-cost of each pollutant.

Discussion

This paper has examined the effect of piracy on the global shipping industry. First, we documented the avoidance behavior that shippers adopt in response to reported pirate encounters. Then, we link these responses to individual adjustments along a route, before deriving the implied aggregate effects (comprising both private costs and public environmental damages). While our estimated adjustment costs may seem relatively small at the individual level, cumulatively they translate to a significant economic loss in the aggregate. Taking the total flow of global shipping routes into account, together with the prevalence of pirate encounters in some of the world's busiest shipping channels, we find that piracy avoidance likely constitutes a considerable cost to the shipping industry. Moreover, avoidance is also an overlooked but material source of environmental externalities.

The simple economic intuition underlying our analysis suggests that ships adjust their voyages to reduce the chance of pirate encounters. But those adjustments do not necessarily mean a complete change of routes (i.e., start and end countries remain the same). This intuition holds up well in the data, where we observe short-lived localized avoidance behavior, which in turn implies higher operational and environmental costs. Each additional encounter amplifies this behavioral response.

As we have tried to emphasize, the Gulf of Aden is something of an outlier in our results. The effects that we observe here are an order of magnitude larger than elsewhere, even other piracy hotspots. Why would the Gulf of Aden present such a different level of adjustment? One possibility is salience and the prominence that these assaults, particularly from Somali pirates, have gained in the public perception. In addition, these responses likely reflect the geographical characteristics of the region, which allow bigger margins of spatial adjustment, though not necessarily through systematic macro-level path adjustment such as switching between crossing the Gulf of Aden or circling around the Cape of Good Hope (see Supplementary Note 4). Unlike vessels destined for Nigeria that must traverse the Gulf of Guinea, or vessels constrained by the narrow straits of Southeast Asia, the open waters of the Gulf of Aden allow captains the physical space to execute larger lateral path deviations to mitigate risk without entirely abandoning their chosen corridor. Implicit in this logic, however, is the assumption that responses are well-approximated by a continuous, linear adjustment in encounter intensity. We view this as appropriate within the range of risk observed in the data, but emphasize that sufficiently elevated risk could in principle produce more discrete or non-linear responses (e.g., systematic corridor switching or canceled trips) that our estimates do not capture.

Such regional heterogeneity notwithstanding, we emphasize that the effect is clear and consistent across space and when measured at the voyage level. The consistency of the results from the two approaches here highlights a global problem for the maritime shipping industry. However, it also underscores the potential for piracy to have wider impacts that ripple across the global economy. We can posit several channels through which these wider impacts manifest. The first is a simple waste of capital. Because individual shippers implement avoidance measures, they must allocate capital to cover these actions. Such capital could have been used somewhere else, either in the form of additional voyages, or as an input to other productive activities.

A second channel is through environmental impacts. The adjustments to piracy are not emission-neutral. In the aggregate, maritime commerce remains a significant source of pollutant emissions, with direct contributions to both global greenhouse emissions and local air pollutants that are harmful to human health and may disproportionately affect different areas and populations[24].

A third channel for wider economic impacts is the potential for indirect trade costs. Depending on the level of competitiveness of the affected industry, and the routes in question, the associated costs in transportation could simultaneously affect both producers and consumers. Previous studies have tried to explore this problem using a trade framework[12,13], and we believe that our approach of examining individual voyages helps further clarify some of the mechanisms behind previously identified trade effects, both at a local and a global scale.

Importantly, we note that these global cost estimates should be interpreted as conservative. Our methodology only captures rerouting of vessels already in transit. Cancelled voyages, temporal and modal substitution to air or land freight, and private security expenditures are all unobservable to us, each of which would increase the total cost incurred as a response to piracy. Similarly, because of our priority for high quality observations, we are removing millions of noisy voyages that might otherwise contribute to the aggregate totals.

On the environmental side, our baseline analysis values carbon damages at $51 per ton following the 2016 Interagency Working Group estimate[25]. More recent estimates place this figure substantially higher (e.g., Rennert et al.[27] suggest \$185 per ton), which would increase the carbon-related component of our damages by a factor of 3.6. We also note that our monetization of local pollutants (NO_x and SO_x) applies a single global damage rate per ton, which does not account for the fact that health damages vary by location. As a partial correction, we restrict the monetization of these pollutants to emissions occurring within national Exclusive Economic Zones and Territorial Seas, which account for 86.09% and 22.82% of the total, respectively.

Stepping back, three key insights derive from our results. First, the piracy problem remains prevalent at a global scale. Second, the sheer density of shipping voyages, particularly in piracy hotspots, means that individual avoidance behaviors accumulate into economically meaningful costs in the aggregate. These losses not only reflect the direct impact on trade flows and transportation inputs, but also the indirect environmental and social costs from pollution. Third, our results highlight the potential value and cost effectiveness of enforcement and anti-piracy measures for piracy-prone areas.

According to available public data[28], a cost-effective defense force could be deployed for roughly US\$330 million per year, adjusted for inflation. Enforcement spending would thus cost a fraction of the almost US\$800 million that we estimate is currently being lost due to piracy on a yearly basis.

We note, however, that the deployment of naval assets or other enforcement measures is not emission-neutral. While likely lower than the emissions resulting from the mass avoidance of the commercial fleet, the environmental cost of these countermeasures should be weighed against their benefits. A typical patrol frigate consumes roughly 40 tons of fuel per day[29], while larger assets like an Arleigh Burke-class destroyer can consume nearly 99 tons per day[30]. Yet, even these significant single-source emissions are likely dwarfed by the aggregate emissions resulting from the mass rerouting of thousands of commercial vessels. Furthermore, emerging technologies such as Unmanned Surface Vessels (USVs) offer the potential for continuous surveillance and deterrence with a significantly lower environmental footprint than traditional naval assets[31]. Addressing this missing enforcement will require coordination and active cooperation from multiple sectors and nations. The benefits, however, could be enjoyed widely.

Alternatively, resources could be directed toward addressing the underlying conditions that give rise to piracy, particularly poverty and limited economic opportunity in affected coastal regions. Public-private partnerships aimed at poverty alleviation and local development may prove to be a cost-effective complement, or alternative, to direct enforcement in reducing piracy risk. Evaluating the design, implementation, and effectiveness of such interventions is an important avenue for future research.

Methods

Data

We construct two unique datasets for global shipping and piracy. Specifically, we compile two panel datasets from 2012 to 2023 that include shipping vessel activity as well as pirate encounters: a spatially gridded and aggregated at $0.5°\times 0.5°$ dataset, and a voyage-level dataset. Each panel covers all global valid cargo and tanker voyages between 2012 and 2023. For the voyage-level dataset, each voyage entry includes reporting vessel characteristics (i.e., type, size, crew), departure and arrival dates, departure and arrival ports and countries, total distance traveled (km), time traveled (hr), speed (km hr^{-1}), fuel consumption (kg), fuel and labor cost (US$), and emissions of CO_2, NO_x, and SO_x (kg).

Shipping activity

Individual shipping vessel activity data come from Global Fishing Watch (GFW), which provides Automatic Identification System (AIS) data that is composed of high-resolution timestamped latitude and longitude messages which are received through satellite, terrestrial, and dynamic receivers[32]. We used the latest version of the GFW data processing pipeline, Version 3[17], which builds on the original AIS data processing methods from[32] and expands coverage from fishing vessels to all types of vessels that carry AIS (including cargo and tanker vessels). AIS transponders are required on all vessels greater than 300 gross registered tons while operating on international voyages, and by many countries while operating in certain exclusive economic zones[33]. The dataset from 2012-2023 includes over 114,000 unique known cargo, tanker, and reefer types as defined by vessel identification data provided by GFW. We use the GFW vessel classification algorithm, which leverages publicly available registry information where available and machine learning algorithms where not available, to include only those vessels that are classified by GFW as one of *cargo*, *cargo* or *tanker*, *bunker* or *tanker*, *tanker*, *cargo* or *reefer*, *specialized reefer*, *container reefer*, *reefer*, or *bunker*.

The GFW data report more than 16 billion individual AIS messages between 2012 and 2023, which we then aggregate into the gridded and voyage-level datasets. Using GFW's dataset of ports and its associated port visit algorithm, we assign every single AIS message to a specific port-to-port trip by a specific vessel[34]. We define a voyage as a single trip between two consecutive port calls. Multi-segment journeys involving intermediate stops are thus treated as a series of individual voyages. We filter the data to only include voyages with reliable profiles: i) total distance traveled and hours spent each greater than zero; ii) total voyage time less than or equal to 60 days; iii) total distance traveled less than or equal to the earth's circumference (40,075 km); iv) total distance traveled less than or equal to four-times the average observed distance for each port-to-port combination; v) departure and arrival countries are known; vi) the total distance traveled is equal or greater than the projected straight-line distance between the starting and ending port; and vii) the vessel has a realistic design speed greater than 10 knots (see below). This process yields 27,760,550 unique valid voyages between 2012 and 2023.

To construct the gridded dataset, we overlay a $0.5° \times 0.5°$ grid on the ocean surface and calculate, for each cell-day, the total occupancy time (hours), distance traveled (km), number of unique vessels, and number of voyages transiting through the cell. We restrict this panel to the 618 grid cells that experienced at least one pirate encounter during the study period.

For the voyage-level regression analysis, we restrict the sample to cargo vessels that transit at most one piracy hotspot and for which complete weather information is available. The weather requirement accounts for the reduction in sample size to 22.9 million voyages.

Shipping operational costs

For our voyage-level dataset, we calculate operational costs from two sources: fuel consumption and labor. We calculate fuel consumption using main engine power, gross tonnage, auxiliary engine power, and design speed. Main engine power and gross tonnage come from the Global Fishing Watch vessel characteristics database[32]. For each vessel, we determine these characteristics using a hierarchy based on data availability: 1) the official registered information of the vessel; and 2) values inferred by the Global Fishing Watch vessel characteristic neural network when available. Auxiliary power is a function of main engine power, and is calculated using known empirical relationships[35], which link main propulsion requirements with vessel characteristics and auxiliary needs. Design speed is a function of main engine power and gross tonnage based on the regression results from[35]. Since this regression can sometimes lead to abnormally low design speed values, we limit our voyage-level analysis to only those vessels for which we calculate an estimated design speed above 10 knots.

Using these vessel characteristics, we calculate fuel consumption using a standard approach that combines fuel consumed by both the main and auxiliary engines[36]. Fuel consumption of the main engine is defined by hours of operation, main engine power, main engine specific fuel consumption rates[37], and a cubic law of operational speed relative to design speed. Fuel consumption of the auxiliary engine is defined by operating hours, auxiliary engine power, and auxiliary engine specific fuel consumption rates[37]. Fuel consumption was calculated for each individual AIS ping, which was then summed across pings for each voyage.

Daily fuel price data come from Bunker Index. We use the 380 CST Bunker Index, which is the global average price from all ports selling 380 centistoke fuel, the most commonly used fuel in maritime transport. Although there is some spatial variation in bunker fuel price across different ports, these regional price data are not available to us. For dates with missing price data within this time range, we impute the missing value using the most recent reported price. Most gaps in the data do not exceed more than two days. Total fuel cost for each voyage is then calculated by multiplying the total fuel consumption of the voyage by the fuel price on the date of departure.

We also keep track of labor requirements and costs for individual voyages. Using the ratio suggested in the literature[35], we estimate the crew needed to operate a vessel as a function of its size and type. The crew wage is calculated using the 2018 International Transport Worker's Federation wage scale for the average non-officer seafarer[38].

Emissions

We also calculate emissions of CO_2, NO_x, and SO_x for each voyage. CO_2 emissions are calculated using a linear relationship[36], which relies on total fuel consumption of the voyage. SO_x emissions are calculated similarly, under the assumption of 3.3% sulfur content for each kilogram of fuel[24]. Similarly, NO_x emissions are calculated using a separate conversion rate for both the main engine fuel consumption (which we assume to be a slow-speed engine) and auxiliary engine (which we assume to be a medium-speed engine)[24].

Weather proxies

Finally, for the voyage-level dataset, we incorporate weather proxies in the forms of average wind speed and direction along each voyage (which we transform into a wind-resistance index that also uses vessel heading), as well as average surface wave height (which is the combined significant height of both wind waves and swell). Both wind and wave height data come from the Copernicus ERA5 reanalysis model[39]. We download monthly data provided at $0.25^\circ \times 0.25^\circ$ resolution.

Mean monthly wind speed, wind direction, and surface wave height information is calculated for $5^\circ \times 5^\circ$ grid cells. For wind speed and wind direction we use a vector averaging approach, in which we first take the individual averages of the u and v vectors of wind speed, and then use those averaged u and v vectors to calculate the average vector wind speed and direction[40]. We take into account wind direction by decomposing the pitch angle relative to the heading of the vessel; the resistance is concave or convex depending on the vessel going against, or with the wind. This measurement is symmetric in absolute terms along each 90° portion of a full circumference and it goes from 0 to 1. Scaling this measurement by the wind speed gives the final wind-resistance index. For each voyage, we calculate the mean wind-resistance and mean surface wave height from across the $5^\circ \times 5^\circ$ pixels that the voyage passed through.

We note that out of the 27,760,550 unique valid voyages between 2012 and 2023, 4,863,686 have missing weather information. This difference then implies that the global sample for our main specification is only 22,896,864.

Pirate encounters

We operationalize pirate encounters using data from the United States National Geospatial Intelligence Agency, which records the dates and locations of sightings and hostile acts against ships by pirates, robbers, and other aggressors[41]. To restrict attention to events that could plausibly influence shipping behavior, we manually reviewed the written description of every encounter between 2012 and 2023 and removed those that occurred in or near ports, took place in inland waterways, were associated with military operations, were not actually aggressive or violent, or could not be confirmed. Each description was reviewed independently by two readers. The disagreements were resolved by a third reader to reach a consensus of 2 out of 3. The resulting dataset contains 2,611 confirmed encounters from 2012–2023.

We then bin encounters into two global grids: a fine $0.5° \times 0.5°$ grid used in the grid-level analysis, and a coarse $5° \times 5°$ grid used in the voyage-level analysis (at the equator, a $5° \times 5°$ cell spans roughly 345×345 miles, a plausible spatial scale for routing or speed decisions in response to recent encounters; a vessel moving at 10 knots can traverse it in about 30 hours). For each grid we compute, for every cell-day, the number of encounters in the cell on that day and the number of days since the most recent encounter in the cell. The 0.5° grid yields the indicator D_{it} used in the grid-level event study (Equation 1). For grid-level robustness, we replicate the same construction at $0.1° \times 0.1°$ and $1° \times 1°$ (Supplementary Note 5).

For the voyage-level analysis we construct three families of encounter indicators that vary in what risk information they assume the captain has at the time of departure. Each family is computed at three pixel resolutions (3°, 5°, 7°); the 5° version is the primary measure and the others are robustness checks. The families of indicators are as follows:

1. **Own-voyage exposure.** For each voyage we count the unique prior encounters that occurred within the exact set of pixels the voyage transited, over rolling windows ending on the departure date. We use windows of 7, 15, and 30 days for the main lag specifications. We also record the number of days since the most recent encounter anywhere along the voyage's pixels.
2. **Route-history exposure (average).** For each voyage on a given port-to-port route, we compute the average number of unique encounters on *previous* voyages along the same route, over 7-, 15-, and 30-day rolling windows.
3. **Route-history exposure (total).** For the same port-to-port route, we compute the total (summed) number of unique encounters across *previous* voyages over the same 7-, 15-, and 30-day windows.

Families (2) and (3) condition on past voyages, so they capture the risk environment a captain would infer from recent traffic on her own route rather than the in-voyage exposure measured by family (1).

Using the locations of all 2,611 encounters, we identify hotspots of pirate activity by density-based clustering[42] with a reachability distance of 10 and a minimum cluster size of 150. Three hotspots emerge over 2012–2023: the Gulf of Aden, the Gulf of Guinea, and Southeast Asia. For each hotspot, we draw a rectangular bounding box snapped to the nearest 5° latitude/longitude markers that fully encloses its encounters. Each 0.5° grid cell and each voyage is then flagged for which hotspot (if any) it falls within or transits through.

The final overlap of shipping voyages and pirate encounters used in the voyage-level analysis is shown in Fig. 1. Encounters concentrate in a small number of corridors—most prominently the Gulf of Guinea, the coast of East Africa, the Arabian Sea, and the jurisdictional waters of the Philippines and Malaysia—with the three relevant hotspots for this study enclosed by the colored rectangles.

Empirical analysis

Grid-level analysis

To establish the effect of piracy on shipping we will rely on several procedures. First, we begin by generally asking if shipping transit is affected by pirate encounters. The analysis is performed under an Eulerian framework, with the units of analysis as grid cells along a $0.5° \times 0.5°$ grid. In particular, we are interested in how measures of shipping traffic over space (i.e., occupancy time, total distance traveled within a grid cell, number of voyages and vessels crossing a grid cell) change following a pirate encounter. Summary statistics for these data are provided in Supplementary Table 1.

We implement this analysis using a within-cell event study design to examine the dynamic response of shipping traffic to pirate encounters. We estimate the following regression model for grid cell i at time t:

$$y_{it} = \sum_{k=-7,k\neq-1}^{7} \beta_k D_{it}^k + \eta_{i,m(t)} + \tau_t + \epsilon_{it} \tag{1}$$

Here, y_{it} is the outcome of interest in grid cell i at time t, and has been inverse-hyperbolic-sine-transformed. The key variables of interest are a set of event-time dummy variables, D_{it}^k.

Each dummy D_{it}^k equals one if grid i at time t is k days relative to a pirate event (e.g., $k = -7$ is 7 days prior, $k = 7$ is 7 days after). A pirate event is a cluster of pirate encounters that occur within a 14-day window.

β_k captures the average marginal change in traffic k days before or after a pirate event, relative to the omitted baseline period one day before the event. The identification assumption is that the timing of an encounter is exogenous to contemporaneous shocks in shipping traffic, after controlling for the comprehensive set of grid and time fixed effects. The model includes grid-cell-by-calendar-month fixed effects ($\eta_{i,m(t)}$), where $m(t)$ denotes the calendar month of date t. These fixed effects absorb all time-invariant differences across cells as well as cell-specific seasonality in shipping activity, which is particularly relevant for maritime traffic patterns that respond to local monsoon cycles, trade-wind regimes, and seasonal demand. The model also includes a full set of date fixed effects (τ_t), which flexibly absorb any shock common to all grid cells on a given day—including global macroeconomic conditions, commodity-price movements, holidays, and day-of-week cycles. We estimate Conley standard errors with a 50 km cutoff[43]. This analysis restricts the sample to grid cells with at least one encounter during our analysis window (2012-2023; 618 grid cells and 1,960 pirate events for a total of 32,129 observations). Our analyses drop singleton observations and observations where the outcome is not available (e.g., when the outcome of interest is distance per vessel, but there were no vessels).

Voyage-level analysis

Building on the grid-level analysis, we then analyze the effect of piracy at the voyage level. We are interested in the feature of a given voyage i (i.e., distance, duration, and speed) along country-to-country route, r, at time t, and their associated consequences in terms of operational costs and emissions. The model is as follows:

$$y_{irt} = \alpha + \beta TNE_{rt} + \delta_i VC_i + \lambda_i W_i + \eta_r R_i + \theta' X_t + \epsilon_{irt} \tag{2}$$

y is the response variable, and TNE is the total number of encounters during the last seven days, with β as the average marginal effect of an additional encounter on the mean path of a voyage. VC is a vector of fixed effects according to vessel characteristics (i.e., type of vessel and size), while W is the time-weighted mean wind-resistance index, average wind speed, and average wave height for a given voyage. Finally, R is a vector of fixed effects by route, while X_t is a battery of month by year fixed effects.

In the results, we will also specifically control for additional factors such as crossing hotspots or the voyage being part of the most common port-to-port combination between countries. To account for potential route and temporal correlation, we cluster standard errors by country-to-country route by year.

Data Availability

Pirate encounter data are publicly available from the US National Geospatial-Intelligence Agency Anti-Shipping Activity Messages database at `https://msi.nga.mil/Piracy`. Vessel tracking data derived from the Automatic Identification System are available from Global Fishing Watch (`https://globalfishingwatch.org`) subject to user registration and the Global Fishing Watch data license. Weather covariates (wind speed and wave height) come from the publicly available Copernicus ERA5 reanalysis (`https://www.ecmwf.int/en/forecasts/dataset/ecmwf-reanalysis-v5`). Daily bunker fuel prices are proprietary and were obtained from Bunker Index (`https://bunkerindex.com`); access requires a paid subscription.

Code Availability

All code used to construct the analysis dataset, run the regressions, and generate the figures and tables in this paper is openly available at `https://github.com/renatomolinah/piracy-shipping`. The repository contains the full data-processing pipeline (managed with the `targets` R package and a Make-based DAG), the BigQuery SQL queries used to aggregate the raw AIS data, and the R scripts that produce every empirical result reported in the main text and Supplementary Information.

References

[1] Asariotis, R. *et al.* Review of maritime transport, 2017. Tech. Rep., United Nations Conference on Trade and Development (2017).

[2] Anderson, J. L. Piracy and world history: an economic perspective on maritime predation. *J. World Hist.* 175–199 (1995).

[3] Gosse, P. *The History of Piracy* (Courier Corporation, 2012).

[4] Bahadur, J. *The Pirates of Somalia: Inside Their Hidden World* (Vintage, 2011).

[5] Bueger, C. Practice, pirates and coast guards: the grand narrative of Somali piracy. *Third World Q.* **34**, 1811–1827 (2013).

[6] Kamal-Deen, A. The anatomy of Gulf of Guinea piracy. *Nav. War Coll. Rev.* **68**, 93–118 (2015).

[7] Hallwood, P. & Miceli, T. J. An economic analysis of maritime piracy and its control. *Scott. J. Polit. Econ.* **60**, 343–359 (2013).

[8] Combined Maritime Forces. Combined task force 151: counter-piracy (2024). `https://combinedmaritimeforces.com/ctf-151-counter-piracy`. Accessed April 2026.

[9] European Union Naval Force. EU NAVFOR Somalia – Operation ATALANTA (2024). `https://eunavfor.eu`. Accessed April 2026.

[10] Maritime Global Security. Best management practices to deter piracy and enhance maritime security in the Red Sea, Gulf of Aden, Indian Ocean and Arabian Sea. Tech. Rep., Maritime Global Security (2025). `https://www.maritimeglobalsecurity.org/media/lx4jmieu/bmp-ms-2025-final-hi-res.pdf`. BMP-MS 2025.

[11] United Nations Security Council. Resolution 2500 (2019). S/RES/2500 (2019). `https://digitallibrary.un.org/record/3838110`.

[12] Bensassi, S. & Martínez-Zarzoso, I. How costly is modern maritime piracy to the international community? *Rev. Int. Econ.* **20**, 869–883 (2012).

[13] Burlando, A., Cristea, A. D. & Lee, L. M. The trade consequences of maritime insecurity: evidence from Somali piracy. *Rev. Int. Econ.* **23**, 525–557 (2015).

[14] Besley, T., Fetzer, T. & Mueller, H. The welfare cost of lawlessness: evidence from Somali piracy. *J. Eur. Econ. Assoc.* **13**, 203–239 (2015).

[15] Sandkamp, A., Stamer, V. & Yang, S. Where has the rum gone? The impact of maritime piracy on trade and transport. *Rev. World Econ.* **158**, 751–778 (2022).

[16] Office of Naval Intelligence. Worldwide threats to shipping (WWTS) reports (2025). `https://t.ly/frrm6`. Accessed: 2025-11-06.

[17] Global Fishing Watch. New release in our AIS data pipeline (version 3) (2024). `https://globalfishingwatch.org/faqs/2024-aug-new-release-in-our-ais-data-pipeline-version-3/`. Accessed: 2025-07-21.

[18] National Geospatial-Intelligence Agency. Worldwide threats to shipping report, 04 Jul 2013 (2013). `https://msi.nga.mil/api/publications/download?key=16920958/SFH00000/wwtts_20130704100000.txt`. Accessed: 2025-11-06.

[19] Quispe, A. *et al.* DIDmultiplegtDYN: estimation in difference-in-difference designs with multiple groups and periods (2026). R package version 2.3.1. `https://CRAN.R-project.org/package=DIDmultiplegtDYN`.

[20] International Maritime Organization. Guidelines for the onboard operational use of shipborne AIS: Resolution A.917(22) (2001). `https://wwwcdn.imo.org/localresources/en/KnowledgeCentre/IndexofIMOResolutions/AssemblyDocuments/A.917(22).pdf`. Accessed: 2025-11-07.

[21] Wang, S. & Meng, Q. Sailing speed optimization for container ships in a liner shipping network. *Transp. Res. E Logist. Transp. Rev.* **48**, 701–714 (2012).

[22] Faber, J. *et al.* Fourth International Maritime Organization greenhouse gas study (2020). International Maritime Organization, London.

[23] Zhang, Y., Eastham, S. D., Lau, A. K. H., Fung, J. C. H. & Selin, N. E. Global air quality and health impacts of domestic and international shipping. *Environ. Res. Lett.* **16**, 084055 (2021).

[24] Corbett, J. J. & Fischbeck, P. Emissions from ships. *Science* **278**, 823–824 (1997).

[25] Interagency Working Group on Social Cost of Greenhouse Gases (United States Government). Technical support document: social cost of carbon, methane, and nitrous oxide interim estimates under Executive Order 13990 (2021). Online.

[26] Mier, M., Adelowo, J. & Weissbart, C. Taxation of carbon emissions and local air pollution in intertemporal optimization frameworks with social and private discount rates (2021). Working paper. `https://www.ifo.de/DocDL/wp-2021-360-mier-adelowo-weissbart-social-cost-air-pollution-carbon.pdf`.

[27] Rennert, K. *et al.* Comprehensive evidence implies a higher social cost of CO2. *Nature* **610**, 687–692 (2022).

[28] Sonnenberg, D. C. *Maritime Law Enforcement: A Critical Capability for the Navy*. Ph.D. thesis, Naval Postgraduate School, Monterey, California (2012).

[29] Work, F. W. *Opportunities for Improved Warship Energy Efficiency: A Canadian Patrol Frigate's Operational Energy Use Patterns* (Harvard University, 2016).

[30] Davey, K. Ship component in hull optimization. *Mar. Technol. Soc. J.* **39**, 39–46 (2005).

[31] Wu, W., Sun, Q. & Yang, H. The application of unmanned vehicle systems during the course of maritime law enforcement. *Front. Mar. Sci.* **12**, 1672951 (2025).

[32] Kroodsma, D. A. *et al.* Tracking the global footprint of fisheries. *Science* **359**, 904–908 (2018).

[33] McCauley, D. J. *et al.* Ending hide and seek at sea. *Science* **351**, 1148–1150 (2016).

[34] Global Fishing Watch. Anchorages, ports and voyages data (2021). `https://globalfishingwatch.org/datasets-and-code-anchorages/`.

[35] Betz, S. *Reducing the Risk of Vessel Strikes to Endangered Whales in the Santa Barbara Channel*. Ph.D. thesis, University of California, Santa Barbara (2011).

[36] Corbett, J. J., Wang, H. & Winebrake, J. J. The effectiveness and costs of speed reductions on emissions from international shipping. *Transp. Res. D Transp. Environ.* **14**, 593–598 (2009).

[37] Wang, C., Corbett, J. J. & Firestone, J. Modeling energy use and emissions from North American shipping: application of the ship traffic, energy, and environment model. *Environ. Sci. Technol.* **41**, 3226–3232 (2007).

[38] International Transport Workers' Federation. ITF Seafarers – wages and compensation (2025). `https://www.itfseafarers.org/en/resources/wages`. Accessed: 2025-11-06.

[39] Hersbach, H. *et al.* The ERA5 global reanalysis. *Q. J. R. Meteorol. Soc.* **146**, 1999–2049 (2020).

[40] Grange, S. K. Technical note: averaging wind speeds and directions (2014). Working paper, University of York.

[41] National Geospatial-Intelligence Agency. Anti-shipping activity messages (ASAM) database (2024). `https://msi.nga.mil/Piracy`. Accessed: 2025-11-06.

[42] Ester, M., Kriegel, H.-P., Sander, J. & Xu, X. A density-based algorithm for discovering clusters in large spatial databases with noise. In *Proc. 2nd Int. Conf. on Knowledge Discovery and Data Mining (KDD)*, 226–231 (1996).

[43] Conley, T. G. GMM estimation with cross sectional dependence. *J. Econom.* **92**, 1–45 (1999).

[44] Rubin, A. P. The law of piracy. *Int. Law Stud.* **63**, 13 (1988).

[45] Gray, T. Turkish piracy and early Stuart Devon. *Rep. Trans. Devonshire Assoc.* **121**, 161 (1989).

[46] Scammell, G. V. European exiles, renegades and outlaws and the maritime economy of Asia c. 1500–1750. *Mod. Asian Stud.* **26**, 641–661 (1992).

[47] Andrews, K. R. *The Spanish Caribbean: Trade and Plunder, 1530–1630* (Yale University Press, New Haven, 1978).

[48] Warren, J. F. *The Sulu Zone, 1768–1898: The Dynamics of External Trade, Slavery, and Ethnicity in the Transformation of a Southeast Asian Maritime State* (NUS Press, 2007).

[49] Tenenti, A. *Piracy and the Decline of Venice, 1580–1615* (University of California Press, 1967).

[50] Wright, R. Piracy set to escalate shipping costs. *Financial Times* (2008). 20 November 2008.

[51] Bowden, A., Hurlburt, K., Aloyo, E., Marts, C. & Lee, A. *The Economic Costs of Maritime Piracy* (One Earth Future Foundation, 2010).

[52] O'Connell, R. J. & Descovich, C. M. Decreasing variance in response time to singular incidents of piracy in the Horn of Africa area of operation. Tech. Rep., Naval Postgraduate School, Monterey, CA, Department of Information Sciences (2010).

[53] Guha, B. & Guha, A. S. Pirates and traders: some economics of pirate-infested seas. *Econ. Lett.* **111**, 147–150 (2011).

[54] Liss, C. Privatization of maritime security in Southeast Asia. In *Private Military and Security Companies*, 135–148 (Springer, 2007).

[55] Flückiger, M. & Ludwig, M. Economic shocks in the fisheries sector and maritime piracy. *J. Dev. Econ.* **114**, 107–125 (2015).

[56] Axbard, S. Income opportunities and sea piracy in Indonesia: evidence from satellite data. *Am. Econ. J. Appl. Econ.* **8**, 154–194 (2016).

[57] Leeson, P. T. An-arrgh-chy: the law and economics of pirate organization. *J. Polit. Econ.* **115**, 1049–1094 (2007).

[58] Psarros, G. A., Christiansen, A. F., Skjong, R. & Gravir, G. On the success rates of maritime piracy attacks. *J. Transp. Secur.* **4**, 309 (2011).

[59] Bahadur, J. Deadly waters: inside the hidden world of Somalia's pirates. In *U.S. Naval Institute Proceedings*, vol. 137, 73–74 (2011).

[60] CNN. Piracy threat returns to African waters (2023). `https://t.ly/qKlZo`. Accessed: 2025-11-06.

[61] ICC International Maritime Bureau. Piracy and armed robbery against ships: report for the period 1 January – 31 December 2017. Tech. Rep., International Maritime Bureau of the International Chamber of Commerce (2018).

[62] The Wire. Abduction of crew off Nigeria brings piracy back to Indian agenda (2023). `https://t.ly/gVVXJ`. Accessed: 2025-11-06.

[63] Time. Pirates in Southeast Asia: the world's most dangerous waters (2023). `https://t.ly/Ano8q`. Accessed: 2025-11-06.

[64] Kiss, A. Maritime piracy in the modern era in Latin America: discrepancies in the regulation. *Acta Hispanica* 121–128 (2020).

[65] United Nations. Report of the Secretary-General on the situation in Haiti (2024). `https://rb.gy/6rku6u`. Accessed: 2025-11-06.

[66] Welch, H. *et al.* Hot spots of unseen fishing vessels. *Sci. Adv.* **8**, eabq2109 (2022).

[67] de Chaisemartin, C. & D'Haultfœuille, X. Difference-in-differences estimators of intertemporal treatment effects. *Rev. Econ. Stat.* 1–45 (2024).

[68] Tominaga, Y. Exploring the economic motivation of maritime piracy. *Def. Peace Econ.* **29**, 383–406 (2018).

Acknowledgements

We thank Christopher Costello, Anca Cristea, Javier Birchenall, Kyle Meng, Olivier Deschenes, Owen Liu, and Christopher Severen for helpful comments on the paper. We are grateful for excellent research assistance provided by J'nesse Balknan, Sebastian Bernhard, Ariella Duvel, Felipe Muschel, and Alejandro Storper. We also acknowledge valuable feedback from participants at the Econometrics Lunch and the Environmental Lunch at the University of California at Santa Barbara (UCSB), the Workshop in Environmental Economics and Data Science at the University of Oregon, and the Summer Conference of the Association of Environmental and Resource Economics. We thank Global Fishing Watch for providing the data processing and data management infrastructure for the shipping data. We would also like to thank Google for providing in-kind computational support.

Partial funding for this project was provided by the Research Provost Award at the University of Miami, the Latin American Fisheries Fellowship at the University of California Santa Barbara, the Chilean Government through the Becas Chile program, and the Environmental Markets Lab at the University of California, Santa Barbara.

Author Contributions

Conceptualization was performed by R.M, J.C.V.D., G.McDo., and G.McDe. Data curation was performed by R.M, J.C.V.D., and G.McDo. Formal Analysis was performed by R.M and J.C.V.D. Funding acquisition was performed by R.M. Investigation was performed by R.M, J.C.V.D., and G.McDo. Methodology was performed by R.M, J.C.V.D., G.McDo., and G.McDe. Project administration was performed by R.M. Supervision was performed by R.M. Validation was performed by R.M, J.C.V.D., G.McDo., and G.McDe. Visualization was performed by R.M., J.C.V.D. and G.McDo. Writing – original draft was written by R.M, J.C.V.D., G.McDo. Writing – review & editing was performed by R.M, J.C.V.D., G.McDo., and G.McDe.

Competing Interests

The authors declare no competing interests.

Supplementary Information for:

The Economic and Environmental Cost of Pirate Avoidance

Renato Molina, Juan Carlos Villaseñor-Derbez,
Gavin McDonald & Grant McDermott

Supplementary Note 1: Background on global piracy

Piracy and trade

Modern piracy is fundamentally an enforcement problem that can be traced to poorly defined property rights and duties over maritime territory. This misalignment is especially acute in international settings, where the establishment and enforcement of anti-pirate regulations usually conflicts with sovereign rights[44]. These institutional settings reduce the probability of pirates being prosecuted, or even apprehended, which in equilibrium encourages the continued predation of sea commerce.

From a welfare perspective, Anderson suggests several types of losses associated with piracy[2]. First, the direct capital losses to violence, which manifest either in the form of damages to the ship or cargo, or as the loss of life. Second, the indirect losses in the form of resources channeled toward evasion and protection that could have been used for other productive activities. For example, the additional bulk of fuel used to maintain evasive maneuvers, or the additional amount of capital required to sustain a steady flow of goods *vis-á-vis* the same exchanges in the absence of piracy. It follows that the magnitude of these responses can lead to both intensive and extensive margin adjustments, which in turn can cause dynamic losses in the form of diminished incentives for producers and merchants to continue with or expand production[2].

Historical data suggest that piracy events have often been followed by significant negative impacts to commerce channels and local economies. For example, during the seventeenth century, the "Turkish pirates" completely paralyzed several parts of west England[45]. During the same period, the predominance of pirate organizations in the Arabian sea also led to severe decreases in trade flow, with devastating consequences for all industries in the region[46]. These two cases are not unique. Similar links have been documented for other trade regions in the Caribbean[47], the Philippines[48], and Venice[49]. All of these examples illustrate how thriving economies suffer considerable negative effects due to piracy.

Modern piracy has had similar effects. In fact, piracy remains a problem worldwide. There were over 2,600 pirate encounters globally between 2012 and 2023, with almost 900 taking place between 2019 and 2023. Most encounters, however, take place in a few hotspots; namely: the Gulf of Aden (known for the Somali pirates), the Gulf of Guinea (mostly within the Nigerian

EEZ), the Malacca Strait (the shipping channel formed by Sumatra and the Malay peninsula) and the South China Sea. For the remainder of the paper we will refer to both the Malacca Strait and the South China Sea as one group that we call Southeast Asia. The distribution of the actual number of encounters in each region over time is shown in Supplementary Fig. 1. From this figure, note that pirate encounters are consistently concentrated in the African region and Southeast Asia.

Although sparse, there are several assessments regarding the economic impact of modern piracy. Past estimates suggest that the losses in trade volume due to pirate activities in Somalia accrued to about \$24 billion per year[13]. Other estimates are more conservative and suggest that the loss ranged between \$1 billion and \$16 billion, when accounting for the addition of 20 days per voyage due to re-routing around Africa, and increased insurance, charter rates, and inventory costs[50–52]. Another study estimates that 10 additional hijacks in either the Gulf of Aden or the Strait of Malacca reduce the volume of exports between Asia and Europe by about 11%, with an estimated cost of about \$25 billion per year[12].

While this literature primarily estimates losses through the examination of aggregate trade flows, there are notable exceptions that look closer at the micro-level. Besley et al.[14] analyze dry bulk shipping contracts and estimate an industry welfare loss of nearly \$3.7 billion, though their pricing-based approach yields little to no evidence of physical re-routing behavior. More recently, Sandkamp et al.[15] use firm-level customs and regionally aggregated AIS data to show that piracy induces a modal shift toward air freight alongside a drop in overall ship density. However, because these studies rely on static contracts or regional aggregation, they cannot trace actual vessel adjustments. To the best of our knowledge, there is no study observing the continuous, physical behavior of individual shipping vessels to quantify the indirect evasion and fuel costs identified by Anderson[2]. We believe tracking these behavioral responses is key to disentangling the true, bottom-up cost of piracy. It is plausible that this gap in the literature is due to the difficulty of obtaining high-frequency tracking data on millions of individual voyages, as well as the sparse data on pirate activities. Both of these issues are accounted for in this paper.

On the other hand, theoretical insights regarding the piracy problem can be traced to two studies. Namely, Guha and Guha[53], who model optimal patrolling and penalties under the option of self-insurance, and Hallwood and Miceli[7], who explore optimal patrolling and penalties taking into account strategic interactions between pirates and shippers. Although very valuable contributions in terms of formalizing the theory behind pirate behavior, neither paper explored vessel adjustments along shipping routes as they focus on penalties and enforcement.

Other related literature has devoted efforts to several topics on both past and modern piracy. One of those topics relates to anti-piracy efforts. Anderson[2] documents the historical evolution of state and individual actions to control for piracy along shipping routes. Similarly, Liss[54] describes how modern piracy incentivizes shippers to employ private military companies or acquire their own defense mechanisms. Other empirical settings, including Flückiger and Ludwig[55], as well as Axbard[56], study how poor fishing conditions lead to an increase in pirate activity in Africa and Indonesia, respectively.

Finally, other authors such as Leeson[57] and Psarros, Christiansen, and Skjong[58] study the factors that contribute to pirates being more or less effective in terms of finding vessels, as well as extracting the most value out of these encounters. In addition and specific to the Somali case, O'Connell and Descovich[52] and Bahadur[59] document the social and economic institutions associated with pirate activities by identifying ransom procedures, operational supply chains, and community support.

The business model of modern piracy

Establishing how pirates operate globally presents several challenges. First, pirates often have little or no incentive to make the details of their operations known to the public. Nonetheless, there are still a few credible sources that allow us to establish the mechanics behind pirate encounters, and more importantly, use them as means for identification in the empirical section. In particular, we make use of the information documented by Bahadur[4], which relies on a number of interviews with individuals who claimed to be associated, directly or indirectly, with pirates in Somalia in 2009. Considering the sensitivity of the piracy issue, these interviews provide the best available information on the actual behavior and incentives of pirates.

Pirates in Somalia appear to not discriminate between vessels. Instead they opportunistically hijack vulnerable vessels that cross their path. Once the potential target is identified, pirates pursue the vessel until eventually capturing it, or the vessel is realistically out of reach. Neither the search nor the pursuit is constrained by the jurisdictional boundaries of Somalia. The boarding strategy entails the pirate crew splitting into several skiffs, which approach the target vessel from all sides while waving and firing their weapons to scare the ship's crew. If the vessel stops, or the skiffs are able to keep up with it, the pirates would toss rope ladders onto the deck and then proceed to boarding. According to the accounts, crews rarely resist boarding once the pirates successfully get on the deck. The average reported success rate of the pirates used to be about 20 to 30%[4].

Once the pirates successfully take control of the ship, they steer the vessel to a friendly port. At this location, an additional set of guards and translators would board the ship, and ransom negotiations will start. Most ransoms would be handled by insurance companies. Upon reaching an agreement, the money is usually delivered via parachute drop-off onto the deck of the ship, and then split among the pirates. The amount that each of them would receive is a fixed fraction of the total ransom, and it would vary depending on the task[4]. About half of the pot would go to the actual men boarding the ship, one third to the investors financing the operation, and a sixth to everyone else assisting with logistics and enforcement.

We note that although 2017 saw a spike in pirate activities in the Gulf of Aden, this region seems to be no longer affected at the same scale as it used to be during the 2000s[60]. According to the latest reports on encounters by the US government (Supplementary Fig. 1**b**) and the International Maritime Bureau of the International Chamber of Commerce (ICC-IMB), most encounters are now reported to take place in the Gulf of Guinea and Southeast Asia[61]. The business model of piracy in these regions, however, differs from the Somali pirates.

Pirates in the Gulf of Guinea follow a similar approach when it comes to intercepting a vessel. The difference comes after they have successfully hijacked the ship. Specifically, besides hijacking the vessel and its crew, these pirates appear to focus on kidnapping only a subset of crew members for ransom[61]. Another regular practice in this region is the robbery of cargo, especially liquid fuel[62].

Pirate encounters in Southeast Asia seem to follow a variation of the previous business model. According to recent reports, and in addition to the practices listed above, encounters include large-scale and sophisticated operations targeted at siphoning fuel from tanker vessels[63]. In this type of attack, vessels are also approached and hijacked, but then they are steered towards a siphoning facility on the shore that retrieves the entire cargo. Under this model, the crew and the ship are usually freed several days after a successful encounter[61].

Finally, pirate and armed-robbery encounters have increased along the Venezuelan and northern Colombian coasts, especially in areas such as the near-shore islands of Venezuela[64]. Economic distress in Venezuela (and parts of northern Colombia) is a key driver, where opportunistic offenders target private yachts and pleasure craft, frequently boarding to seize cash, groceries, electronics and other easily carried valuables. To date these incidents appear generally sporadic and focused on smaller craft rather than large cargo vessels or full-scale hijackings. In the broader Caribbean there have been instances of commercial ship boarding, kidnapping of crewmembers, or ransom demands near Haiti[65].

Supplementary Note 2: Regression analysis

In this section, we provide supporting material for the regression analyses referenced in the study. First, we provide the tables with the summary statistics for the data used in the grid and voyage regressions, respectively. Supplementary Table 1 shows that the average traffic per grid is highly variable across the globe, with the Gulf of Aden and Southeast Asia having much higher distance, occupancy time, voyages and unique vessels transiting in their respective areas than the rest of the world combined. For example, the average daily occupancy is about 40 and 140 hours in the Gulf of Aden and the Southeast Asia hotspots, respectively, while in the rest of the world the daily occupancy is 31 hours. This pattern persists for all the variables in the dataset, though there is considerable spread among all sub-samples and variables.

Supplementary Table 2 shows that when analyzed at the voyage level, the pattern is slightly modified. Here, on average, vessels crossing hotspots travel longer distances and spend more time at sea than vessels not crossing through hotspots, though there is also a relatively high degree of spread on the voyage features. Importantly, the hotspots with the highest mean observed piracy encounters in the preceding three months along routes take place in the Gulf of Guinea. The distribution of the remaining variables in the analysis (i.e., costs and emissions) follows directly from these observed features.

Second, Supplementary Table 3 documents the spatial persistence of piracy. That is, the probability that, conditional on an attack in a given $0.5^{\circ} \times 0.5^{\circ}$ grid cell, at least one additional attack occurs in the same cell within a specified time window. In the Gulf of Aden, spatial recurrence is low: only 13.6% of encounters are followed by another attack in the same cell within 7 days, rising modestly to 17.1% within 30 days. This pattern is consistent with opportunistic, open-ocean encounters that do not cluster tightly in space. In Southeast Asia, recurrence is substantially higher (27.1% within 7 days, 48.8% within 30 days), consistent with territorial piracy concentrated in narrow corridors.

Third, we provide the regression tables not presented in the main text. The results for the linear average effect of piracy on fuel, labor, and total operational costs (in thousands of US dollars) are stacked in Supplementary Table 4. Across all samples, the results show that path adjustments increase fuel cost the most. One additional encounter relates to hundreds or thousands of dollars in additional fuel spent. These estimates are consistent with path adjustments. The results also suggest that vessels passing through the Gulf of Aden face the biggest burden with an additional US$11 thousand per encounter, while those in the Gulf of Guinea face the least.

These adjustments are also meaningful in terms of labor cost. The effects of additional encounters are positive and significant, but at most half of the adjustment cost when compared to additional fuel consumption. We note that this result is consistent across samples.

We estimate the effect of piracy on total operational costs by aggregating both fuel and labor costs. These results are reported in Panel (C) of Supplementary Table 4, and suggest that the average increase in operational costs due to avoidance measures per additional pirate encounter ranges from over US$1,100 in the Gulf of Guinea to over US$10,000 in the Gulf of Aden. Globally, this effect averages down to about US$2,300 for each additional pirate encounter.

Finally, the linear average effects of piracy on emissions are stacked in Supplementary Table 5 for CO_2, NO_x, and SO_x, respectively. As expected from previous results, excessive fuel consumption leads to excessive emissions across the spectrum of relevant pollutants. In particular, increases in CO_2 range from 5 to 46 tons per voyage per past pirate encounter. NO_x and SO_x emissions due to piracy are relatively less voluminous, though this is a direct consequence of their significantly smaller concentrations in bunker fuel relative to carbon. Nonetheless, regression estimates point to hundreds of kilograms, and tons in the case of the Gulf of Aden, of excess pollutants emitted due to the presence of pirates.

Supplementary Table 1: Summary Statistics for Daily Ship Transit by Grid Cell.

	Distance (km)	Occupancy (hr)	Voyages (#)	Unique vessels (#)
Gulf of Aden				
Mean	972.4	40.2	16.9	16.8
SD	1,098.8	46.4	20.9	20.7
P5	0.0	0.0	0.0	0.0
P95	3,127.6	129.2	58.0	58.0
Gulf of Guinea				
Mean	161.9	14.3	4.1	4.1
SD	175.0	18.6	3.9	3.8
P5	0.0	0.0	0.0	0.0
P95	524.7	53.1	12.0	12.0
Southeast Asia				
Mean	2,352.2	139.8	47.7	46.9
SD	3,292.0	178.4	70.6	69.9
P5	0.0	0.0	0.0	0.0
P95	9,416.4	504.3	213.0	210.0
Rest of the World				
Mean	398.3	31.4	9.9	9.6
SD	680.6	47.4	15.7	15.4
P5	0.0	0.0	0.0	0.0
P95	1,829.4	117.0	35.0	35.0

The unit of observation is a grid cell-day on a $0.5° \times 0.5°$ grid. The sample includes 618 grid cells with at least one pirate encounter during the 2012–2023 period. Each column reports a different measure of daily shipping activity within a cell. P5 and P95 denote the 5th and 95th percentiles, respectively.

Supplementary Table 2: Summary Statistics for Individual Voyage Features.

	Voyage Features			Encounters (#)		
	Distance (km)	Time (hr)	Speed (km h^{-1})	7 days	15 days	30 days
Gulf of Aden						
Mean	1,906.1	96.1	19.7	0.1	0.1	0.3
SD	2,883.1	142.9	6.9	0.3	0.5	0.8
P5	35.7	2.4	6.9	0.0	0.0	0.0
P95	6,864.1	342.0	30.7	0.0	1.0	2.0
Gulf of Guinea						
Mean	3,376.8	161.2	20.5	0.3	0.7	1.4
SD	3,947.6	190.1	6.8	0.8	1.3	2.2
P5	40.4	3.5	8.2	0.0	0.0	0.0
P95	11,062.1	519.1	31.6	2.0	3.0	6.0
Southeast Asia						
Mean	1,361.5	70.0	18.1	0.2	0.3	0.7
SD	2,733.7	132.5	6.4	0.6	1.1	2.0
P5	8.2	0.5	8.3	0.0	0.0	0.0
P95	6,591.6	311.2	29.6	1.0	2.0	5.0
Rest of the World						
Mean	826.4	40.8	19.8	0.0	0.0	0.0
SD	1,711.8	80.5	6.5	0.1	0.1	0.2
P5	4.7	0.3	9.4	0.0	0.0	0.0
P95	3,117.9	162.2	31.3	0.0	0.0	0.0

The unit of observation is a voyage. The sample includes all cargo vessel voyages from 2012 to 2023 that pass through at most one piracy hotspot. Voyage features report total distance (km), total time (hr), and average speed (km h^{-1}). Encounters report the count of pirate encounters recorded in the projected path of the vessel using a 5-degree spatial footprint over the preceding 7, 15, and 30 days, respectively. P5 and P95 denote the 5th and 95th percentiles, respectively.

Supplementary Table 3: Spatial Persistence of Pirate Encounters.

Window	Global	Gulf of Aden	Gulf of Guinea	Southeast Asia
Within 1 day	9.9%	11.6%	9.1%	13.2%
Within 7 days	18.5%	13.6%	14.2%	27.1%
Within 15 days	25.8%	15.5%	20.5%	37.2%
Within 30 days	34.5%	17.1%	28.0%	48.8%

Each cell reports the probability that, conditional on an attack occurring in a $0.5° \times 0.5°$ grid cell, at least one additional attack occurs in the same cell within the specified time window. Sample: 2,611 encounters from 2012–2023. Hotspot assignment uses the bounding boxes described in the main text.

Supplementary Table 4: Effect of Past Pirate Encounters on Shipping Cost.

	Global	G. of Aden	G. of Guinea	S.E. Asia
Panel (A): Fuel Cost (thousands of US$)				
Encounters (7 day)	1.94***	9.36***	0.72***	1.48***
	(0.24)	(1.12)	(0.20)	(0.28)
Panel (B): Labor Cost (thousands of US$)				
Encounters (7 day)	0.35***	1.26***	0.43***	0.25***
	(0.03)	(0.17)	(0.04)	(0.03)
Panel (C): Total Cost (thousands of US$)				
Encounters (7 day)	2.29***	10.62***	1.14***	1.72***
	(0.26)	(1.24)	(0.21)	(0.30)
Observations	22,896,864	888,075	316,716	4,560,514
Hotspot FE	X	•	•	•

* $p < 0.1$, ** $p < 0.05$, *** $p < 0.01$ The unit of observation is a voyage. Estimates are from Equation (2). Each panel examines a calculated cost in terms of fuel cost, labor cost, and total cost as the sum of both. All coefficients are in thousands of US$. Each column is a different sample: Global uses the full sample; G. of Aden, G. of Guinea, and S.E. Asia restrict to voyages passing through each hotspot, respectively. Encounters (7 day) is the count of pirate encounters recorded in the projected path of the vessel in the preceding 7 days from the departure date using a 5-degree spatial footprint. The sample spans from 2012 to 2023. Controls include average wind speed, the wind-resistance index, and average wave height along the voyage. Fixed effects include country-to-country combination, vessel type, vessel size, hotspot, top route, and month-by-year. X indicates the fixed effect is included; • indicates the fixed effect is absorbed by the sample restriction. Standard errors are clustered by country-to-country route by year.

Supplementary Table 5: Effect of Past Pirate Encounters on Shipping Emissions.

	Global	G. of Aden	G. of Guinea	S.E. Asia
Panel (A): CO2 (tons)				
Encounters (7 day)	7.93***	46.34***	7.31***	5.03***
	(0.84)	(6.01)	(0.79)	(0.79)
Panel (B): NOx (kg)				
Encounters (7 day)	198.92***	1196.77***	181.38***	124.48***
	(21.83)	(155.70)	(20.49)	(20.50)
Panel (C): SOx (kg)				
Encounters (7 day)	165.11***	964.76***	152.26***	104.73***
	(17.58)	(125.21)	(16.37)	(16.42)
Observations	22,896,864	888,075	316,716	4,560,514
Hotspot FE	X	•	•	•

* $p < 0.1$, ** $p < 0.05$, *** $p < 0.01$ The unit of observation is a voyage. Estimates are from Equation (2). Each panel examines a calculated emission in terms of CO_2 (tons), NOx (kg), and SOx (kg). Each column is a different sample: Global uses the full sample; G. of Aden, G. of Guinea, and S.E. Asia restrict to voyages passing through each hotspot, respectively. Encounters (7 day) is the count of pirate encounters recorded in the projected path of the vessel in the preceding 7 days from the departure date using a 5-degree spatial footprint. The sample spans from 2012 to 2023. Controls include average wind speed, the wind-resistance index, and average wave height along the voyage. Fixed effects include country-to-country combination, vessel type, vessel size, hotspot, top route, and month-by-year. X indicates the fixed effect is included; • indicates the fixed effect is absorbed by the sample restriction. Standard errors are clustered by country-to-country route by year.

Supplementary Note 3: Counterfactual costs and emissions

We use the fully specified *global* model (5° grid, 7 day window) to predict voyage-level fuel and labor costs, as well as emissions of CO_2, NO_x, and SO_x. We make predictions using the observed number of pirate encounters and a counterfactual of no pirate encounters at all. We then take the difference between these two predictions to obtain a voyage-level estimate of the additional fuel and labor costs, and emissions of each pollutant. We then calculate the total annual costs and emissions across all voyages. These results are shown in Supplementary Table 6 and Supplementary Table 7, where we also provide information disaggregated by hotspot.

Having matched each voyage to its additional costs and emissions, we then divide a voyage's cost (or emissions) across all $0.5° \times 0.5°$ grid cells along which the vessel transited. For each grid cell, we calculate the total excess costs (fuel + labor) or emissions of each pollutant. We then take the average across all years (2012-2023) and use these data to produce maps shown in Supplementary Fig. 4**a**.

We monetize the environmental impacts caused by additional emission of local and global air pollutants using their social cost. Specifically, we use estimates provided by the Interagency Working Group on Social Cost of Greenhouse Gases[25], which suggest that an additional ton of CO_2 or NO_x induce damages valued at US$51 and US$18,000 (in 2020 US$ assuming a 3% discount rate). For SO_x we use estimates from Mier, Adelowo, and Weissbart[26], which indicates an additional ton of SO_2 induces damages of US$14,694 (in 2020 US$). We then aggregate all information by ASAM region, and produce the bar chart shown in Supplementary Fig. 4**e**.

Supplementary Table 6: Total Costs of Piracy to the Shipping Industry.

	2012	2013	2014	2015	2016	2017	2018	2019	2020	2021	2022	2023
Fuel (millions of US$)												
Global	120	179	206	202	133	168	71	105	195	198	229	299
G. of Aden	23	14	8	3	6	22	5	5	9	8	6	9
G. of Guinea	21	23	15	10	22	24	18	13	29	14	7	6
Southeast Asia	67	130	179	178	84	104	32	77	136	161	204	276
Labor (millions of US$)												
Global	20	30	36	35	23	30	13	20	37	39	49	66
G. of Aden	4	2	1	1	1	4	1	1	2	2	1	2
G. of Guinea	4	4	3	2	4	4	3	2	5	3	2	1
Southeast Asia	11	22	31	31	15	19	6	14	26	32	43	61
Total (millions of US$)												
Global	140	209	242	237	157	198	84	125	232	237	278	365
G. of Aden	27	16	9	4	7	26	6	6	10	10	7	11
G. of Guinea	25	27	17	12	25	28	22	16	34	17	9	8
Southeast Asia	78	152	209	208	98	123	38	92	162	193	248	337

Counterfactual costs are derived from the fully specified global voyage-level model (Equation (2), 5-degree grid, 7-day window). For each voyage, we predict operational costs under the observed encounter intensity and under a counterfactual of zero encounters, then take the difference. Fuel costs are calculated using vessel-specific engine characteristics and daily bunker fuel prices. Labor costs are based on crew size (estimated from vessel type and tonnage) and standard seafarer wage rates. All values in 2020 US$. Values are aggregated annually by hotspot region.

Supplementary Table 7: Total Emission of Air Pollutants due to Piracy.

	2012	2013	2014	2015	2016	2017	2018	2019	2020	2021	2022	2023
CO_2 (Thousand metric tons)												
Global	437	659	772	758	506	650	283	424	798	847	1,061	1,439
G. of Aden	85	50	29	13	21	85	20	19	35	36	27	44
G. of Guinea	77	84	56	38	82	92	73	54	119	60	33	31
Southeast Asia	244	478	668	665	317	404	128	312	557	690	945	1,329
NOx (Metric tons)												
Global	10,963	16,541	19,368	19,010	12,704	16,315	7,101	10,648	20,019	21,257	26,620	36,088
G. of Aden	2,125	1,265	739	315	531	2,123	506	480	883	892	680	1,115
G. of Guinea	1,942	2,101	1,398	965	2,059	2,298	1,828	1,348	2,980	1,509	830	767
Southeast Asia	6,126	11,997	16,763	16,691	7,953	10,129	3,217	7,834	13,969	17,320	23,714	33,329
SOx (Metric tons)												
Global	9,099	13,729	16,076	15,778	10,544	13,541	5,894	8,838	16,616	17,643	22,095	29,953
G. of Aden	1,764	1,050	613	261	440	1,762	420	399	733	740	564	925
G. of Guinea	1,612	1,744	1,161	801	1,709	1,907	1,517	1,119	2,473	1,253	689	637
Southeast Asia	5,085	9,957	13,914	13,854	6,601	8,407	2,670	6,502	11,595	14,375	19,683	27,663

Counterfactual emissions are derived from the fully specified global voyage-level model (Equation (2), 5-degree grid, 7-day window). For each voyage, we predict emissions under the observed encounter intensity and under a counterfactual of zero encounters, then take the difference. CO_2 emissions are calculated using a standard linear fuel-to-carbon conversion. NO_x and SO_x emissions are calculated using engine-type-specific emission factors. Values are aggregated annually by hotspot region.

Supplementary Note 4: Extensions

Adjustments in route choice

The main analysis focuses on changes in path and characteristics of observed voyages. As a complementary exercise, we examine whether piracy exposure is also associated with short-run changes in voyage frequency at the route level. To do so, we aggregate the voyage-level data to the weekly country-pair level and estimate a negative binomial count model of weekly departures on recent encounter intensity.

The model is as follows:

$$Y_{rt} \sim \text{NegBin}(\mu_{rt}, \kappa), \qquad \log(\mu_{rt}) = \alpha + \beta \, ANE_{r,t-1} + \gamma_r + \delta_t, \tag{1}$$

where Y_{rt} denotes the number of voyages observed for country-pair route r in week t. $ANE_{r,t-1}$ is the average encounter intensity observed along voyages on route r during the preceding 7-day window. γ_r denotes country-pair fixed effects, and δ_t denotes month-by-year fixed effects. Standard errors are clustered by country-pair and year.

Supplementary Table 8 reports the results. The estimates provide little evidence that piracy exposure produces meaningful short-run adjustments in trip frequency. None of the coefficients reaches the 5% statistical significance level, and the implied magnitudes are small relative to baseline activity. In the Gulf of Aden subsample, where the average country-pair route carries 9.8 trips per week, the point estimate of 0.0156 implies a 1.6% change in weekly trips per unit of average prior encounters, or roughly 0.15 additional trips per week at the 95th percentile of exposure and 0.31 trips per week at the 99th percentile. Together with the fact that 87.5% of Aden route-weeks see zero prior encounters in the preceding week, these patterns indicate that the extensive margin of voyage frequency is not the primary channel through which vessels respond to piracy risk in our data.

Supplementary Table 8: Effect of Pirate Encounters on Trip Frequency.

	Global	G. of Aden	G. of Guinea	S.E. Asia
Avg. Encounters (7-day lag)	0.0054*	0.0156*	-0.0050	-0.0006
	(0.0032)	(0.0088)	(0.0039)	(0.0041)
Observations	968,785	98,564	115,310	114,351
Country-Pair FE	X	X	X	X
Hotspot FE	X	•	•	•
Month-by-Year FE	X	X	X	X

* $p < 0.1$, ** $p < 0.05$, *** $p < 0.01$ The unit of observation is a country-pair by 7-day window. The outcome is the count of cargo vessel trips on that route in that week. The model is Negative Binomial; coefficients are log-multiplicative and approximately equal to percentage changes in trips for small values. The sample spans from 2012 to 2023. Global uses the full sample; G. of Aden, G. of Guinea, and S.E. Asia restrict the sample to routes passing through each hotspot, respectively. Avg. Encounters (7-day lag) is the average of each voyage's 7-day pirate encounter count in the prior 7-day window on the same route, using a 5-degree spatial footprint. This mirrors the 7-day encounter window used in the main voyage-level analysis. Controls include average wind speed, the wind-resistance index, and average wave height. Fixed effects include country-to-country combination, hotspot, and month-by-year. X indicates the fixed effect is included; • indicates the fixed effect is absorbed by the sample restriction. Standard errors are clustered by country-to-country route by year.

Adjustments in the Gulf of Aden: Suez Canal vs Cape of Good Hope

To better understand the pronounced behavioral responses observed in the Gulf of Aden in Supplementary Table 1, we conduct a descriptive corridor-choice analysis focusing on vessels utilizing either the Suez Canal or the Cape of Good Hope corridors. Using our AIS-based voyage records, we identify these voyages, aggregate them at the daily level for the 2012–2023 period, and merge them with daily piracy encounters in the Gulf of Aden.

Supplementary Fig. 1 summarizes the data by plotting i) monthly Gulf of Aden encounters, ii) standardized monthly voyage volumes through the Suez and around the Cape, and iii) the monthly Cape share among all corridor trips. The data reveal some potential substitution between the two corridors, with some of these overlaps following high counts of pirate encounters in the Gulf of Aden.

To examine this route-choice margin, we aggregate corridor traffic to the daily level and estimate the following binomial logit models:

$$\text{Cape}_t \sim \text{Binomial}(\text{Cape}_t + \text{Suez}_t,\ p_t)\,, \qquad \text{logit}(p_t) = \alpha + \beta X_t + \gamma_t + \delta_t + \lambda_t. \tag{2}$$

With Cape_t as the number of corridor trips using the Cape of Good Hope on day t, Suez_t as the number using the Suez Canal, and p_t as the implied probability that a voyage goes around the Cape. X_t represents either i) recent encounter intensity in the Gulf of Aden, measured as the number of encounters in the prior 7, 15, or 30 days, or ii) an indicator for high-encounter (75th percentile or higher) periods over those same windows. γ_t, δ_t, and λ_t denote day-of-week, month, and year fixed effects, respectively, added progressively across specifications. Standard errors are clustered at the month-year level.

Supplementary Table 9 presents the results. There is little evidence of a systematic *shift* from the Suez Canal to the Cape of Good Hope in response to recent piracy encounters in the Gulf of Aden. Across both the continuous encounter measures in Panel (A) and the high-encounter indicators in Panel (B), the estimated coefficients are generally small, imprecise, and statistically indistinguishable from zero. Overall, the table does not reveal a statistically robust corridor-switching response to recent pirate encounters.

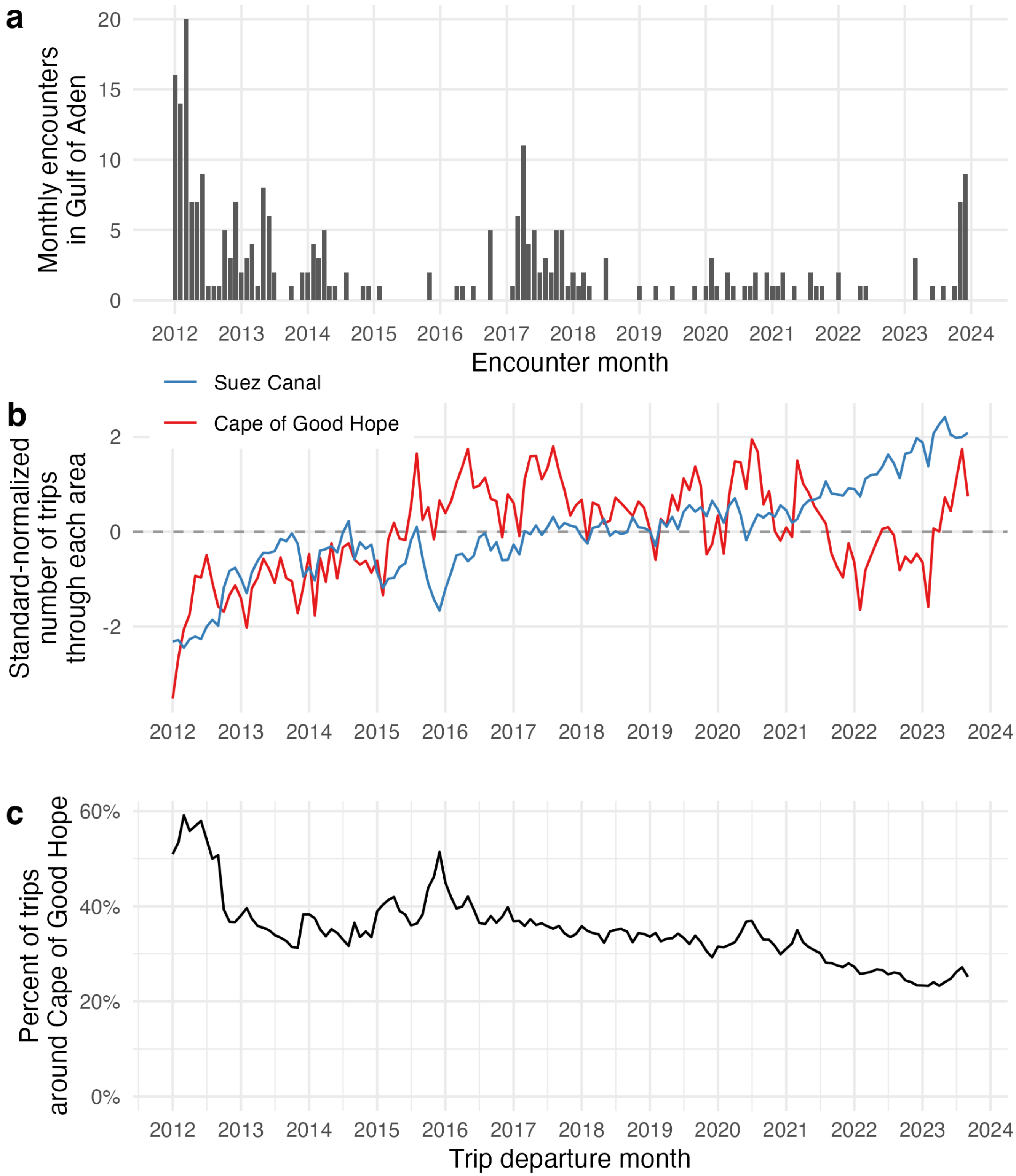

Supplementary Figure 1: **Route use through the Suez Canal and around the Cape of Good Hope, and Gulf of Aden pirate encounters over time.** **a** shows monthly Gulf of Aden pirate encounters. **b** shows standardized monthly trips through the Suez Canal and around the Cape of Good Hope. **c** shows the monthly share of trips that use the Cape route among all trips that use either corridor.

One additional feature is worth noting. There is a sharp reduction in observations once we control for country combinations. This reflects the fact that many origin-destination pairs in the sample consistently use *only* one corridor. We therefore interpret this exercise cautiously. Overall, the trip-level route-choice analysis does not provide strong evidence that recent piracy exposure systematically induces corridor substitution in Aden-related traffic.

Supplementary Table 9: Corridor Choice Between the Suez Canal and the Cape of Good Hope: Trip-Level Evidence.

	(1)	(2)	(3)	(4)	(5)	(6)	(7)	(8)	(9)
Panel (A): Continuous encounter intensity									
Encounters in prior 7 days	-0.001	-0.002	-0.013						
	(0.024)	(0.025)	(0.105)						
Encounters in prior 15 days				-0.023	-0.023	0.082			
				(0.022)	(0.023)	(0.090)			
Encounters in prior 30 days							-0.010	-0.009	0.116
							(0.022)	(0.022)	(0.083)
Panel (B): High-encounter indicator									
High encounters (7d window)	-0.004	-0.003	-0.009						
	(0.054)	(0.055)	(0.266)						
High encounters (15d window)				-0.041	-0.039	0.074			
				(0.066)	(0.066)	(0.239)			
High encounters (30d window)							0.087	0.087	0.307
							(0.095)	(0.096)	(0.271)
Observations	499,882	499,882	64,186	499,882	499,882	64,186	499,882	499,882	64,186
DoW FE		X	X		X	X		X	X
Country Combo. FE			X			X			X
Vessel Type FE		X	X		X	X		X	X
Vessel Size FE		X	X		X	X		X	X
Top Route FE			X			X			X
Weather controls	X	X	X	X	X	X	X	X	X
Month-by-Year FE	X	X	X	X	X	X	X	X	X

* $p < 0.1$, ** $p < 0.05$, *** $p < 0.01$ The unit of observation is an individual vessel trip. The outcome is a binary indicator equal to one if the trip used the Cape of Good Hope route (zero for Suez Canal). The sample spans from 2012 to 2023. Encounters in prior X days is the count of pirate encounters recorded in the Gulf of Aden in the preceding X days from the departure date. Panel B defines high-encounter periods as those above the 75th percentile of the encounter distribution within each window. Columns (2), (5), and (8) add day-of-week, vessel-type, and vessel-size fixed effects. Columns (3), (6), and (9) further add country-pair and top-route fixed effects. Controls include average wind speed, the wind-resistance index, and average wave height. X indicates the fixed effect is included. Standard errors are clustered by month-by-year.

Supplementary Note 5: Robustness tests

This section shows robustness checks for all of the empirical results: how pirate encounters affect total shipping traffic within grid cells, and how pirate encounters relate to features of individual voyages. The two sets of robustness checks largely corroborate the patterns in the main text. Pirate encounters reduce traffic within grid cells. These adjustments imply adjustments at the individual voyage level, which is then corroborated by the strong association between pirate activity and the average total distance and time traveled for the same country-to-country combination.

Grid-level analysis

First, we show that our results are driven by shippers avoiding an area with known presence of pirates rather than by other behavioral adaptations. For example, a shipping captain may decide to disable the AIS transponder onboard their vessel as a way to conceal their presence. To test for this, we use a publicly available dataset of known AIS disabling events. For details on the data, see[66]. Essentially, we match known positions where a vessel "went dark" to all grid cells with at least one reported pirate encounter. As with our main-text specifications, we regress the number of AIS disabling events on a dummy variable indicating whether the day was before or after a reported pirate encounter. Our results are shown in Supplementary Table 10. At a global level, we do not find enough evidence suggesting that the number of AIS-disabling events increases within the 7 days following a pirate encounter. In the Gulf of Aden we retrieve a non-significant and negative coefficient of -0.001. In the Gulf of Guinea we see a moderate increase, with a coefficient of 0.002. This coefficient is also not statistically significant. We do not estimate the effect for the Southeast Asia hotspot because the outcome variable was always 0 (i.e., there were no disabling events within attacked hotspots).

Second, we show that our grid-level results are not driven by choices of the spatial resolution for our analysis. To test for this, we repeat our analysis but this time using two other resolutions. Our main-text results use a $0.5° \times 0.5°$ grid. Supplementary Fig. 2 shows results for two other resolutions. Namely, we increase the spatial resolution to $0.1° \times 0.1°$ or decrease it to $1° \times 1°$. Both resolutions show similar patterns, with the finer grid showing longer lasting and sharper effects than those associated with the coarser grid, as would be expected.

Finally, we apply commonly used estimators for cases with different groups, treatment periods, and when the treatment is non-absorbing[19]. Pirate encounters are a non-absorbing treatment because affected grid cells are not perpetually under piracy, and thus allow shipping activity to eventually resume. This analysis uses the not-yet-treated grid cells to build a counterfactual of expected transit metrics for the cell with an encounter. The estimator is also robust to heterogeneous treatment effects. We restrict the sample to only single-switcher grid cells (i.e., those with only one attack) and estimate 7 placebo and treatment effects to match the $\pm$ 7-day window from our main-text estimates. Event study results are presented in Supplementary Fig. 3. As with our main-text results, we detect that shipping transit significantly decreases within affected grid cells following pirate encounters. The estimates here are twice as large as the ones presented in the main text (e.g., occupancy time decreases by 20%, compared to 9% in the main text Supplementary Fig. 3). Supplementary Table 11 shows the average treatment effects are negative for all outcome variables of interest, in agreement with our main-text analysis. Furthermore, it shows that the joint nullity of the placebos (column p(effects)) are not statistically significant at the 0.05 level, suggesting a lack of pre-trends.

Supplementary Table 10: Effect of Pirate Encounters on AIS Disabling Events.

	Global	G. of Aden	G. of Guinea
Post	0.000	−0.001	0.002
	(0.000)	(0.003)	(0.002)
Observations	31.944	2.413	8.181

* $p < 0.1$, ** $p < 0.05$, *** $p < 0.01$ This table tests whether vessels disable their AIS transponders following a piracy report. The unit of observation is a grid cell-day. Each column represents a different geographic region. The Southeast Asia hotspot is excluded because there were no disabling events detected within pixels with pirate activity. Post is a binary indicator equal to 1 for days on or after a pirate event in the grid cell. The analysis uses a 7-day window around events to identify pre- and post-encounter periods. The sample spans from 2012 to 2023. All regressions include grid-cell-by-month and date fixed effects. Standard errors are Conley standard errors (50 km cutoff) and reported in parentheses.

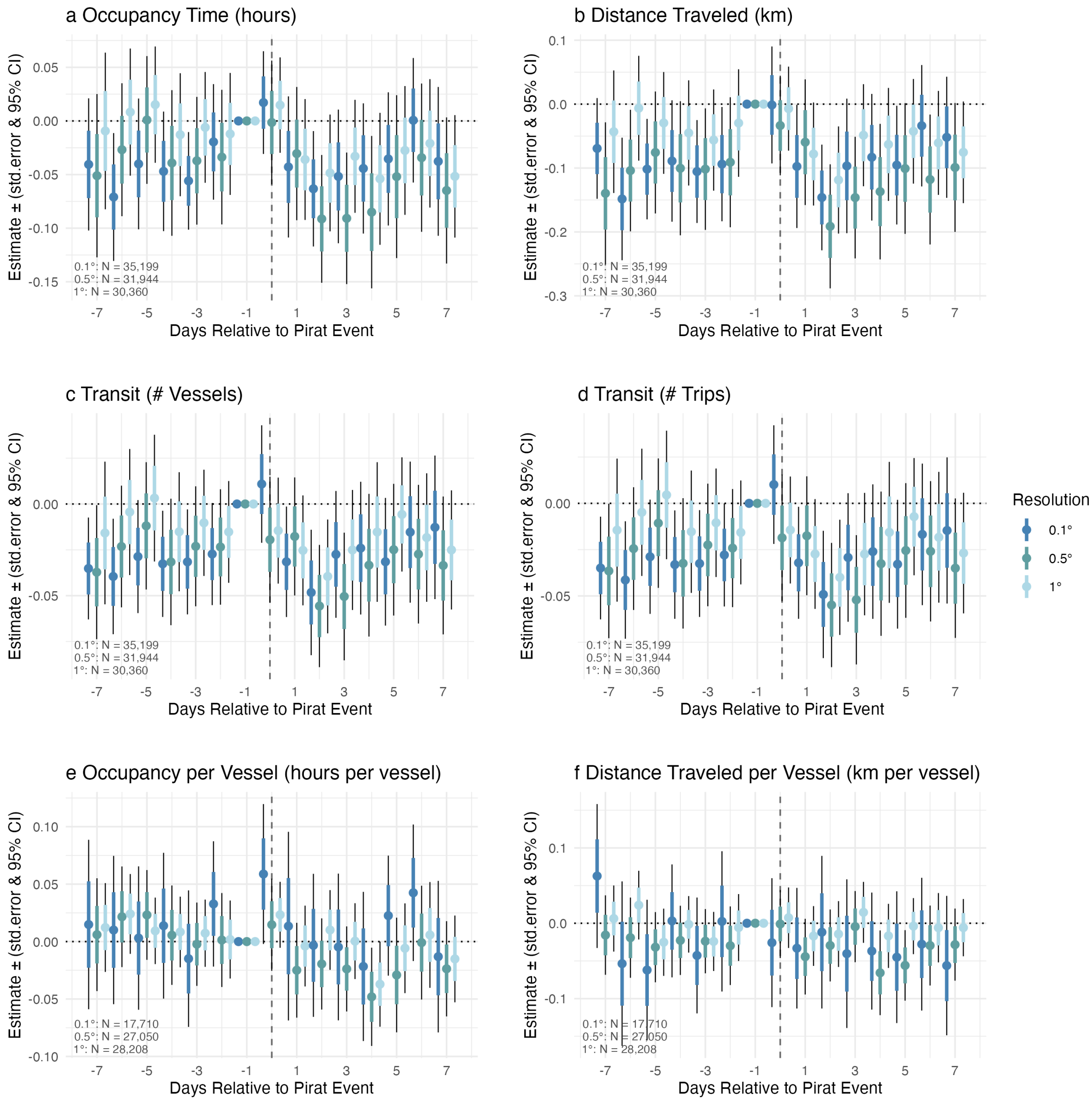

Supplementary Figure 2: **Dynamic effects of piracy on ship transit for three different grid resolutions.** The unit of observation is a grid cell-day. Each inset examines a different shipping activity measure. The horizontal axis shows time relative to the day of the attack. The vertical axis shows the magnitude of the effect. Points are coefficient estimates from Equation (1), showing the change in shipping activity relative to one day before the attack ($k = -1$). Different colors indicate different resolutions. All models include grid-cell-by-month and date fixed effects. The thick portion of error bars shows Conley standard errors (50 km cutoff), and the thin portion shows 95% Confidence Intervals.

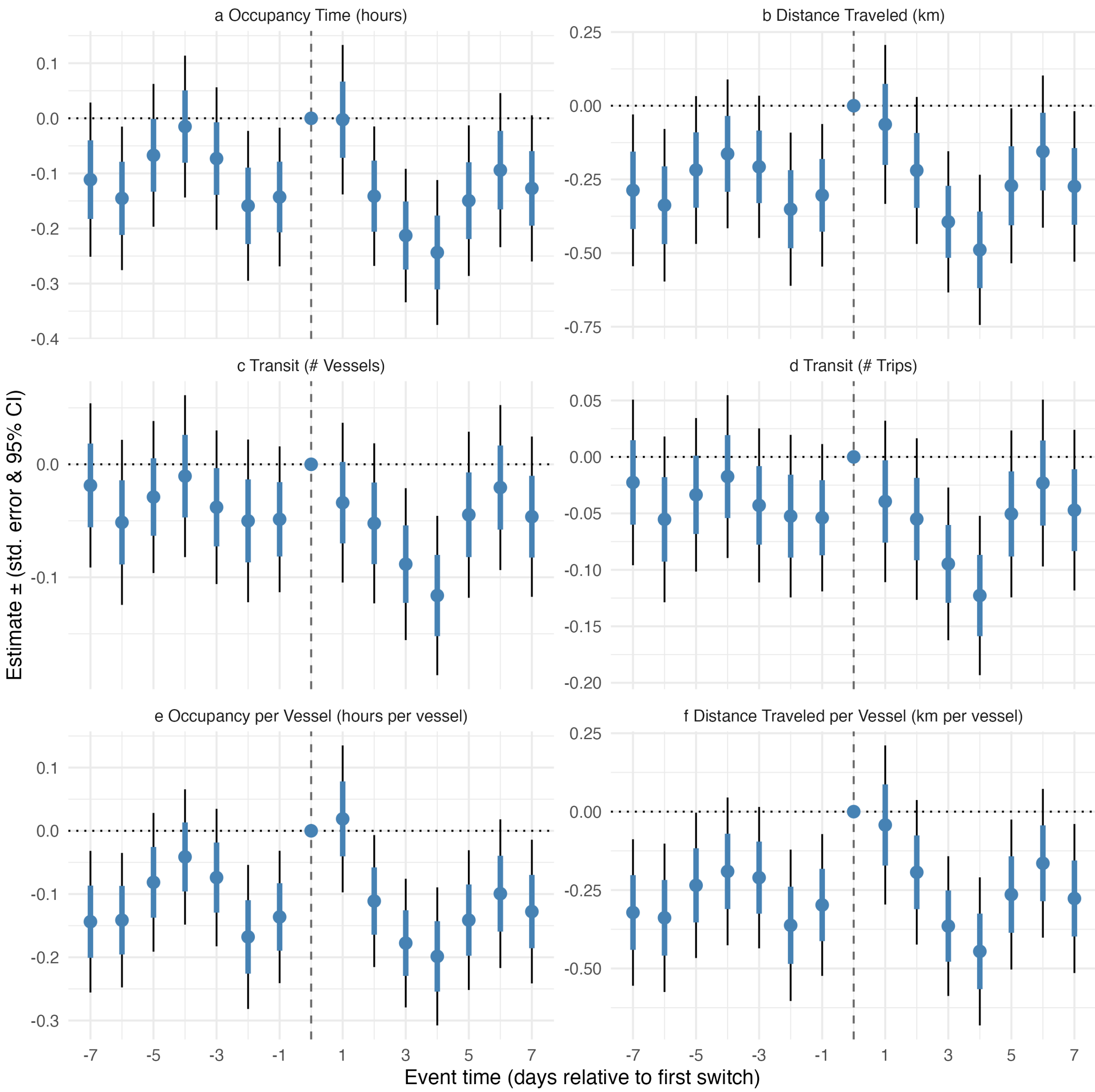

Supplementary Figure 3: **Dynamic effects of piracy on ship transit with heterogeneity-robust estimates**. The unit of observation is a grid cell-day. Each inset examines a different shipping activity measure. The horizontal axis shows time relative to the time of a pirate encounter. The vertical axis shows the magnitude of the effect. Points are coefficient estimates, showing the change in shipping activity relative to one day before the attack. The thick portion of error bars shows standard errors, and the thin portion shows 95% confidence intervals.

Supplementary Table 11: Effect of Pirate Encounters on Grid Cell Shipping Activity.

Outcome	ATE	SE	p (effects)	p (placebos)
Distance Traveled (km)	-1.867	0.705	0.002	0.203
Distance Traveled per Vessel (km per vessel)	-1.752	0.659	0.001	0.116
Occupancy Time (hours)	-0.971	0.364	0.001	0.165
Occupancy per Vessel (hours per vessel)	-0.837	0.312	0.001	0.054
Transit (# Trips)	-0.433	0.193	0.020	0.717
Transit (# Vessels)	-0.402	0.191	0.034	0.742

Each row corresponds to one transformed shipping-activity outcome estimated from the daily grid-cell panel. ATE is the average cumulative effect from DIDmultiplegtDYN and p-values correspond to the joint null tests for post-treatment effects and placebo leads. All regressions use N = 302,106 of which N = 2,534 come from switchers.

Voyage-level analysis

Here we present evidence of the robustness of the voyage analysis to several assumptions. First, we show robustness to different sets of fixed effects in tabular form. The estimates are sensitive to the inclusion of country-to-country fixed effects, but this is expected as the length and specific paths of each route are bound to vary widely across combinations. The suite of results are included in Supplementary Tables 12 to 20. Overall, the results are stable across the addition of vessel, hotspot and top route fixed effects. The results are also robust to the inclusion of weather controls in the form of wind speed, wind-resistance index, and wave height.

Supplementary Tables 12 to 20, column (7), replace country-to-country and top-route fixed effects with port-to-port pair fixed effects. This specification identifies effects from within-port-pair variation across voyages on the same origin-destination connection, and the encounter coefficient attenuates considerably. We interpret the difference between columns (6) and (7) as reflecting both port-pair substitution, which is itself a piracy-response margin absorbed by column (7), and time-invariant geographic differences between port pairs that are unrelated to piracy responses.

Although we cannot fully decompose these channels without additional structure, port-pair substitution appears empirically important. The median country pair is served by 5 distinct port-to-port connections, and the dominant port pair accounts for only ≈13% of voyages on a voyage-weighted basis, implying roughly 17 effective port-pair connections per country pair. Port choice is therefore an active margin available to shippers, and port-pair fixed effects absorb part of the avoidance behavior we seek to measure.

There is also substantial sparsity in port-pair connections. The median port pair has only 2 voyages over the 12-year sample, and only 24.5% have 10 or more voyages. As a result, column (7)'s identifying variation is concentrated in a small subset of dense lanes, limiting its direct comparability with column (6). We therefore retain column (6) as the preferred specification because country-pair fixed effects capture the relevant economic market for bilateral shipping, while preserving within-country port substitution as a response margin. Column (7) is nevertheless informative as a conservative within-port-pair estimate that absorbs port-pair substitution.

We note that almost 5 million voyages are dropped when adding weather controls. This is because spatiotemporal wind speed data is available globally from ERA5. Wind vector data meanwhile, is a composite of both wind speed and vessel heading. Heading is usually, but not always, broadcast during the transmission of AIS messages, meaning that a value for the wind vector cannot be calculated for some voyages where the vessel does not broadcast its heading. Wave height data from ERA5 is restricted to the ocean, meaning that its value may be missing for trips that occurred exclusively within some inland areas such as some rivers and lakes. Wave height data are also limited in areas that are predominantly covered by sea ice, and thus may be missing for trips that occur exclusively in these areas.

Second, we show robustness to i) using rolling windows of 7, 15, and 30 days, and ii) constructing the past-encounters variable using global $3° \times 3°$, $5° \times 5°$, and $7° \times 7°$ grids. This allows us to assess the temporal and spatial sensitivity of the estimates; the results are shown in Supplementary Fig. 4. Across specifications, the effects of recent encounters on distance and travel time generally diminish as longer time windows are considered. Sensitivity to the spatial footprint is also evident, with larger grids often attenuating the estimates, particularly in the global sample, the Gulf of Aden, and Southeast Asia, although this pattern is less uniform in the Gulf of Guinea. For completeness, we maintain these variations in temporal and spatial scale in all of the analyses below.

Third, we show robustness of the results to the categorization of cargo vessels. In the main analysis, we use the best available vessel class for each individual vessel as categorized by Global Fishing Watch. This "best available" approach uses the vessel class provided by official registries where available, and infers vessel class using a neural network when registries are not available[32]. As a robustness check, we restrict the analysis to work with: 1) vessels that are always categorized as cargo vessels according to official registries; as well as 2) expand it as those who are categorized in official registries as being cargo vessels at least once. These results are shown in Supplementary Fig. 5 and Supplementary Fig. 6 and are virtually unchanged with respect to the results in the main analysis, though minimal changes around zero are detected for the speed analysis. We reiterate that the magnitudes detected for speed are practically meaningless.

Fourth, we show robustness to the definition of our explanatory variable. For each voyage, we calculate the total number of unique encounters that occurred along all previously traveled paths (i.e., surrogate trips), as well as the chosen path, for each port-to-port route within the preceding months of a voyage's departure. This represents, for any given voyage departure date for any given port-to-port route, the captain's assessment of the prevalence of piracy along the universe of potential paths that have been recently traveled along the route. We call this variable "Total Number of Encounters." The results from this test are shown in Supplementary Fig. 7 and are consistent with the main analysis, though there is attenuation. This is expected, as the marginal impact of an additional pirate encounter diminishes as the potential area of paths along a route increases.

In addition, for each voyage we calculate the average number of unique pirate encounters that occurred along all previously traveled paths (i.e., surrogate trips) for that port-to-port route within a time window. This represents, for any given voyage departure date for any given port-to-port route, the captain's expectation of how many encounters could occur along the path. We call this variable "Average Number of Encounters." This analysis is presented in Supplementary Fig. 8, and shows considerable attenuation. Positive effects in terms of distance are detected, except in Southeast Asia. Effects in terms of time are mostly dissipated. This result is expected, as it is again easy to see the marginal impact of an additional pirate encounter diminishes further as its effect is now diluted by a considerable increase in the spatial footprint considered, over the number of voyages that took place before.

We also show robustness of the results to the addition of speed and days since the last encounter along a route as *covariates*. The results are shown in Supplementary Fig. 9, and are practically unchanged. These results provide support that the omission of voyage speed or other short-term risk features does not bias the main adjustment estimates.

Supplementary Table 12: Effect of Past Pirate Encounters on Voyage Distance.

	(1)	(2)	(3)	(4)	(5)	(6)	(7)
Encounters (7 day)	972.08***	1,041.06***	56.48***	54.72***	54.05***	54.28***	11.53***
	(78.67)	(68.44)	(4.73)	(4.53)	(4.50)	(4.45)	(0.87)
Wind Speed (m/s)		160.94***	−1.39	−0.59	−4.58*	−3.62	−0.34
		(24.46)	(2.87)	(2.66)	(2.71)	(2.65)	(0.39)
Wind Resistance Index (m/s)		18.25***	0.81*	0.54	0.68	0.79*	−0.45***
		(4.48)	(0.43)	(0.42)	(0.43)	(0.41)	(0.08)
Wave Height (m)		1,120.47***	241.61***	237.97***	219.09***	214.76***	33.60***
		(100.27)	(14.96)	(13.25)	(15.13)	(14.64)	(2.49)
Observations	27,760,550	22,897,792	22,896,864	22,896,864	22,896,864	22,896,864	22,721,524
Country Combo. FE			X	X	X	X	
Vessel Type FE				X	X	X	X
Vessel Size FE				X	X	X	X
Hotspot FE					X	X	X
Top Route FE						X	
Port-to-Port FE							X
Month-by-Year FE	X	X	X	X	X	X	X

* $p < 0.1$, ** $p < 0.05$, *** $p < 0.01$ The unit of observation is a voyage. Estimates are from Equation (2). Each column is a different specification. Encounters (7 day) is the count of pirate encounters recorded in the projected path of the vessel in the preceding 7 days from the departure date using a 5-degree spatial footprint. The sample spans from 2012 to 2023. Controls include average wind speed, the wind-resistance index, and average wave height along the voyage. Column (7) replaces country-to-country and top route fixed effects with port-to-port pair fixed effects. X indicates the fixed effect is included. Standard errors are clustered by country-to-country route by year.

Supplementary Table 13: Effect of Past Pirate Encounters on Voyage Time.

	(1)	(2)	(3)	(4)	(5)	(6)	(7)
Encounters (7 day)	45.50***	47.92***	2.90***	2.83***	2.80***	2.82***	0.89***
	(3.60)	(3.19)	(0.25)	(0.25)	(0.24)	(0.24)	(0.09)
Wind Speed (m/s)		7.47***	−0.37***	−0.38***	−0.56***	−0.49***	−0.24***
		(1.09)	(0.14)	(0.13)	(0.14)	(0.13)	(0.04)
Wind Resistance Index (m/s)		0.00	−0.63***	−0.63***	−0.62***	−0.62***	−0.63***
		(0.18)	(0.04)	(0.04)	(0.04)	(0.04)	(0.03)
Wave Height (m)		46.50***	13.64***	13.54***	12.61***	12.27***	4.74***
		(4.58)	(0.82)	(0.74)	(0.83)	(0.80)	(0.26)
Observations	27,760,550	22,897,792	22,896,864	22,896,864	22,896,864	22,896,864	22,721,524
Country Combo. FE			X	X	X	X	
Vessel Type FE				X	X	X	X
Vessel Size FE				X	X	X	X
Hotspot FE					X	X	X
Top Route FE						X	
Port-to-Port FE							X
Month-by-Year FE	X	X	X	X	X	X	X

* $p < 0.1$, ** $p < 0.05$, *** $p < 0.01$ The unit of observation is a voyage. Estimates are from Equation (2). Each column is a different specification. Encounters (7 day) is the count of pirate encounters recorded in the projected path of the vessel in the preceding 7 days from the departure date using a 5-degree spatial footprint. The sample spans from 2012 to 2023. Controls include average wind speed, the wind-resistance index, and average wave height along the voyage. Column (7) replaces country-to-country and top route fixed effects with port-to-port pair fixed effects. X indicates the fixed effect is included. Standard errors are clustered by country-to-country route by year.

Supplementary Table 14: Effect of Past Pirate Encounters on Voyage Speed.

	(1)	(2)	(3)	(4)	(5)	(6)	(7)
Encounters (7 day)	0.76***	0.69***	0.07***	0.04***	0.04***	0.04***	−0.03***
	(0.11)	(0.09)	(0.01)	(0.01)	(0.01)	(0.01)	(0.01)
Wind Speed (m/s)		−0.03	0.00	0.03**	0.02	0.01	0.00
		(0.06)	(0.02)	(0.01)	(0.01)	(0.01)	(0.01)
Wind Resistance Index (m/s)		0.21***	0.17***	0.17***	0.17***	0.17***	0.18***
		(0.01)	(0.01)	(0.01)	(0.01)	(0.01)	(0.01)
Wave Height (m)		1.78***	0.06	0.02	−0.03	0.00	−0.57***
		(0.19)	(0.10)	(0.07)	(0.07)	(0.07)	(0.03)
Observations	27,760,550	22,897,792	22,896,864	22,896,864	22,896,864	22,896,864	22,721,524
Country Combo. FE			X	X	X	X	
Vessel Type FE				X	X	X	X
Vessel Size FE				X	X	X	X
Hotspot FE					X	X	X
Top Route FE						X	
Port-to-Port FE							X
Month-by-Year FE	X	X	X	X	X	X	X

* $p < 0.1$, ** $p < 0.05$, *** $p < 0.01$ The unit of observation is a voyage. Estimates are from Equation (2). Each column is a different specification. Encounters (7 day) is the count of pirate encounters recorded in the projected path of the vessel in the preceding 7 days from the departure date using a 5-degree spatial footprint. The sample spans from 2012 to 2023. Controls include average wind speed, the wind-resistance index, and average wave height along the voyage. Column (7) replaces country-to-country and top route fixed effects with port-to-port pair fixed effects. X indicates the fixed effect is included. Standard errors are clustered by country-to-country route by year.

Supplementary Table 15: Effect of Past Pirate Encounters on Fuel Cost.

	(1)	(2)	(3)	(4)	(5)	(6)	(7)
Encounters (7 day)	22.02***	23.77***	2.08***	1.96***	1.94***	1.94***	0.94***
	(1.86)	(1.62)	(0.25)	(0.24)	(0.24)	(0.24)	(0.21)
Wind Speed (m/s)		3.67***	0.03	0.12	0.02	0.02	0.04
		(0.55)	(0.09)	(0.09)	(0.09)	(0.09)	(0.07)
Wind Resistance Index (m/s)		0.56***	0.10***	0.07***	0.07***	0.07***	0.09***
		(0.11)	(0.02)	(0.02)	(0.02)	(0.02)	(0.01)
Wave Height (m)		24.84***	4.83***	3.91***	3.48***	3.50***	0.11
		(2.32)	(0.40)	(0.34)	(0.36)	(0.36)	(0.23)
Observations	27,760,550	22,897,792	22,896,864	22,896,864	22,896,864	22,896,864	22,721,524
Country Combo. FE			X	X	X	X	
Vessel Type FE				X	X	X	X
Vessel Size FE				X	X	X	X
Hotspot FE					X	X	X
Top Route FE						X	
Port-to-Port FE							X
Month-by-Year FE	X	X	X	X	X	X	X

* $p < 0.1$, ** $p < 0.05$, *** $p < 0.01$ The unit of observation is a voyage. Estimates are from Equation (2). Each column is a different specification. Encounters (7 day) is the count of pirate encounters recorded in the projected path of the vessel in the preceding 7 days from the departure date using a 5-degree spatial footprint. The sample spans from 2012 to 2023. Controls include average wind speed, the wind-resistance index, and average wave height along the voyage. Column (7) replaces country-to-country and top route fixed effects with port-to-port pair fixed effects. X indicates the fixed effect is included. Standard errors are clustered by country-to-country route by year.

Supplementary Table 16: Effect of Past Pirate Encounters on Labor Cost.

	(1)	(2)	(3)	(4)	(5)	(6)	(7)
Encounters (7 day)	5.94***	6.33***	0.37***	0.36***	0.35***	0.35***	0.10***
	(0.48)	(0.42)	(0.03)	(0.03)	(0.03)	(0.03)	(0.01)
Wind Speed (m/s)		0.88***	−0.06***	−0.05***	−0.08***	−0.07***	−0.03***
		(0.14)	(0.02)	(0.02)	(0.02)	(0.02)	(0.00)
Wind Resistance Index (m/s)		0.02	−0.08***	−0.08***	−0.08***	−0.08***	−0.08***
		(0.02)	(0.00)	(0.00)	(0.01)	(0.00)	(0.00)
Wave Height (m)		6.83***	1.87***	1.84***	1.73***	1.69***	0.62***
		(0.53)	(0.12)	(0.10)	(0.10)	(0.10)	(0.03)
Observations	27,760,550	22,897,792	22,896,864	22,896,864	22,896,864	22,896,864	22,721,524
Country Combo. FE			X	X	X	X	
Vessel Type FE				X	X	X	X
Vessel Size FE				X	X	X	X
Hotspot FE					X	X	X
Top Route FE						X	
Port-to-Port FE							X
Month-by-Year FE	X	X	X	X	X	X	X

* $p < 0.1$, ** $p < 0.05$, *** $p < 0.01$ The unit of observation is a voyage. Estimates are from Equation (2). Each column is a different specification. Encounters (7 day) is the count of pirate encounters recorded in the projected path of the vessel in the preceding 7 days from the departure date using a 5-degree spatial footprint. The sample spans from 2012 to 2023. Controls include average wind speed, the wind-resistance index, and average wave height along the voyage. Column (7) replaces country-to-country and top route fixed effects with port-to-port pair fixed effects. X indicates the fixed effect is included. Standard errors are clustered by country-to-country route by year.

Supplementary Table 17: Effect of Past Pirate Encounters on Total Cost.

	(1)	(2)	(3)	(4)	(5)	(6)	(7)
Encounters (7 day)	27.96***	30.10***	2.45***	2.31***	2.29***	2.29***	1.05***
	(2.32)	(2.03)	(0.26)	(0.26)	(0.26)	(0.26)	(0.21)
Wind Speed (m/s)		4.55***	−0.03	0.06	−0.06	−0.05	0.01
		(0.69)	(0.10)	(0.10)	(0.10)	(0.10)	(0.07)
Wind Resistance Index (m/s)		0.58***	0.02	−0.01	−0.01	−0.01	0.01
		(0.13)	(0.02)	(0.02)	(0.02)	(0.02)	(0.01)
Wave Height (m)		31.67***	6.70***	5.75***	5.21***	5.19***	0.72***
		(2.83)	(0.48)	(0.40)	(0.43)	(0.43)	(0.24)
Observations	27,760,550	22,897,792	22,896,864	22,896,864	22,896,864	22,896,864	22,721,524
Country Combo. FE			X	X	X	X	
Vessel Type FE				X	X	X	X
Vessel Size FE				X	X	X	X
Hotspot FE					X	X	X
Top Route FE						X	
Port-to-Port FE							X
Month-by-Year FE	X	X	X	X	X	X	X

* $p < 0.1$, ** $p < 0.05$, *** $p < 0.01$ The unit of observation is a voyage. Estimates are from Equation (2). Each column is a different specification. Encounters (7 day) is the count of pirate encounters recorded in the projected path of the vessel in the preceding 7 days from the departure date using a 5-degree spatial footprint. The sample spans from 2012 to 2023. Controls include average wind speed, the wind-resistance index, and average wave height along the voyage. Column (7) replaces country-to-country and top route fixed effects with port-to-port pair fixed effects. X indicates the fixed effect is included. Standard errors are clustered by country-to-country route by year.

Supplementary Table 18: Effect of Past Pirate Encounters on CO2 Emissions.

	(1)	(2)	(3)	(4)	(5)	(6)	(7)
Encounters (7 day)	141.88***	153.58***	8.86***	8.05***	7.94***	7.93***	1.70***
	(11.69)	(10.10)	(0.90)	(0.85)	(0.84)	(0.84)	(0.50)
Wind Speed (m/s)		24.15***	−0.01	0.60	0.00	−0.03	−0.01
		(3.68)	(0.43)	(0.43)	(0.42)	(0.42)	(0.07)
Wind Resistance Index (m/s)		3.65***	0.56***	0.35***	0.37***	0.37***	0.51***
		(0.75)	(0.09)	(0.09)	(0.09)	(0.09)	(0.05)
Wave Height (m)		166.79***	32.67***	26.44***	23.76***	23.89***	1.36***
		(15.42)	(2.42)	(1.95)	(2.08)	(2.08)	(0.35)
Observations	27,760,550	22,897,792	22,896,864	22,896,864	22,896,864	22,896,864	22,721,524
Country Combo. FE			X	X	X	X	
Vessel Type FE				X	X	X	X
Vessel Size FE				X	X	X	X
Hotspot FE					X	X	X
Top Route FE						X	
Port-to-Port FE							X
Month-by-Year FE	X	X	X	X	X	X	X

* $p < 0.1$, ** $p < 0.05$, *** $p < 0.01$ The unit of observation is a voyage. Estimates are from Equation (2). Each column is a different specification. Encounters (7 day) is the count of pirate encounters recorded in the projected path of the vessel in the preceding 7 days from the departure date using a 5-degree spatial footprint. The sample spans from 2012 to 2023. Controls include average wind speed, the wind-resistance index, and average wave height along the voyage. Column (7) replaces country-to-country and top route fixed effects with port-to-port pair fixed effects. X indicates the fixed effect is included. Standard errors are clustered by country-to-country route by year.

Supplementary Table 19: Effect of Past Pirate Encounters on NOx Emissions.

	(1)	(2)	(3)	(4)	(5)	(6)	(7)
Encounters (7 day)	3,589.18***	3,890.15***	222.57***	201.96***	199.18***	198.92***	40.90***
	(296.73)	(256.07)	(23.30)	(21.86)	(21.77)	(21.83)	(13.15)
Wind Speed (m/s)		611.60***	1.00	17.02	1.60	0.53	1.53
		(93.66)	(11.02)	(10.97)	(10.79)	(10.86)	(1.76)
Wind Resistance Index (m/s)		99.52***	19.31***	14.01***	14.58***	14.45***	17.70***
		(19.27)	(2.40)	(2.47)	(2.45)	(2.44)	(1.46)
Wave Height (m)		4,269.31***	816.77***	656.36***	588.13***	592.92***	9.74
		(392.68)	(61.88)	(50.07)	(53.24)	(53.52)	(8.91)
Observations	27,760,550	22,897,792	22,896,864	22,896,864	22,896,864	22,896,864	22,721,524
Country Combo. FE			X	X	X	X	
Vessel Type FE				X	X	X	X
Vessel Size FE				X	X	X	X
Hotspot FE					X	X	X
Top Route FE						X	
Port-to-Port FE							X
Month-by-Year FE	X	X	X	X	X	X	X

* $p < 0.1$, ** $p < 0.05$, *** $p < 0.01$ The unit of observation is a voyage. Estimates are from Equation (2). Each column is a different specification. Encounters (7 day) is the count of pirate encounters recorded in the projected path of the vessel in the preceding 7 days from the departure date using a 5-degree spatial footprint. The sample spans from 2012 to 2023. Controls include average wind speed, the wind-resistance index, and average wave height along the voyage. Column (7) replaces country-to-country and top route fixed effects with port-to-port pair fixed effects. X indicates the fixed effect is included. Standard errors are clustered by country-to-country route by year.

Supplementary Table 20: Effect of Past Pirate Encounters on SOx Emissions.

	(1)	(2)	(3)	(4)	(5)	(6)	(7)
Encounters (7 day)	2,954.03***	3,197.59***	184.54***	167.53***	165.26***	165.11***	35.34***
	(243.38)	(210.24)	(18.83)	(17.62)	(17.55)	(17.58)	(10.39)
Wind Speed (m/s)		502.82***	−0.27	12.49	−0.09	−0.73	−0.11
		(76.56)	(8.94)	(8.86)	(8.72)	(8.76)	(1.41)
Wind Resistance Index (m/s)		75.91***	11.63***	7.32***	7.78***	7.71***	10.69***
		(15.53)	(1.86)	(1.91)	(1.90)	(1.90)	(1.05)
Wave Height (m)		3,472.50***	680.13***	550.46***	494.63***	497.49***	28.24***
		(321.11)	(50.40)	(40.64)	(43.29)	(43.41)	(7.25)
Observations	27,760,550	22,897,792	22,896,864	22,896,864	22,896,864	22,896,864	22,721,524
Country Combo. FE			X	X	X	X	
Vessel Type FE				X	X	X	X
Vessel Size FE				X	X	X	X
Hotspot FE					X	X	X
Top Route FE						X	
Port-to-Port FE							X
Month-by-Year FE	X	X	X	X	X	X	X

* $p < 0.1$, ** $p < 0.05$, *** $p < 0.01$ The unit of observation is a voyage. Estimates are from Equation (2). Each column is a different specification. Encounters (7 day) is the count of pirate encounters recorded in the projected path of the vessel in the preceding 7 days from the departure date using a 5-degree spatial footprint. The sample spans from 2012 to 2023. Controls include average wind speed, the wind-resistance index, and average wave height along the voyage. Column (7) replaces country-to-country and top route fixed effects with port-to-port pair fixed effects. X indicates the fixed effect is included. Standard errors are clustered by country-to-country route by year.

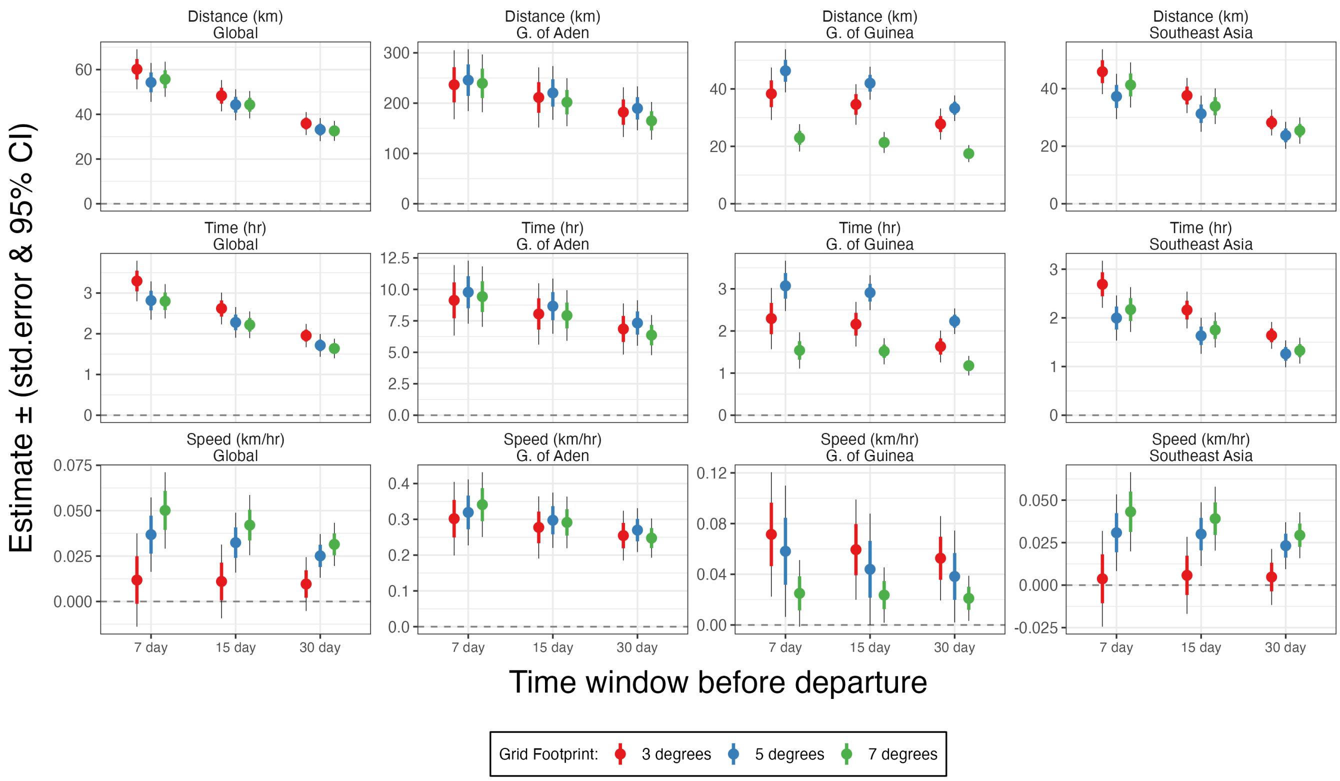

Supplementary Figure 4: **Replication Under Different Time Horizons and Degree Footprints.** Coefficient estimates from Equation (2) show the change in voyage features as a function of the number of pirate encounters along the voyage path in the preceding months. Each plot shows the results for models using time windows of 7, 15, and 30 days, respectively. Each color shows results for models using a 3, 5, and 7° spatial footprint, respectively. The thick portion of error bars shows clustered standard errors, and the thin portion shows 95% Confidence Intervals. Estimation, subsampling, specification, and clustering approach remain identical to those in Supplementary Table 1.

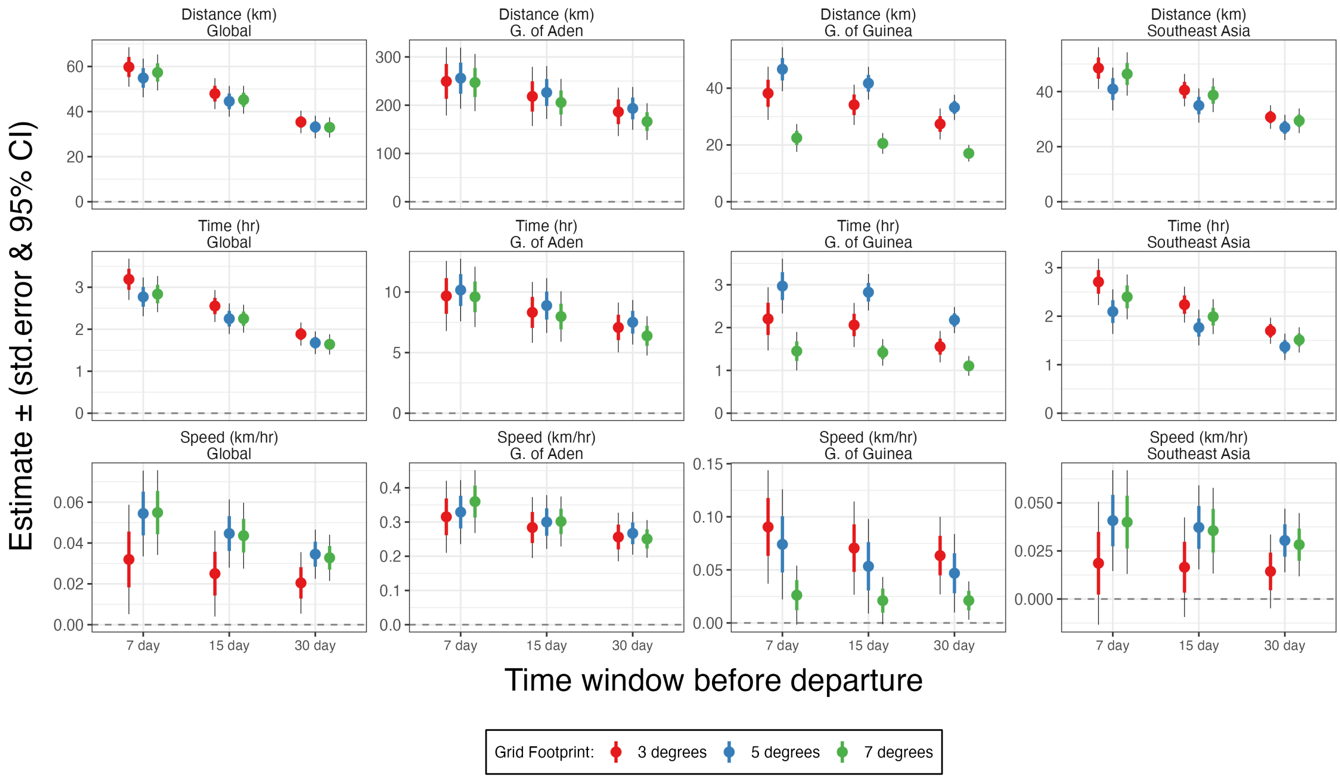

Supplementary Figure 5: **Replication Under Different Time Horizons and Degree Footprints of Vessels Always Classified as Cargo.** Coefficient estimates from Equation (2) show the change in voyage features as a function of the number of pirate encounters along the voyage path in the preceding months. The sample is restricted to vessels always classified as cargo by official registries. Each plot shows the results for models using time windows of 7, 15, and 30 days, respectively. Each color shows results for models using a 3, 5, and 7° spatial footprint, respectively. The thick portion of error bars shows clustered standard errors, and the thin portion shows 95% Confidence Intervals. Estimation, subsampling, specification, and clustering approach remain identical to those in Supplementary Table 1.

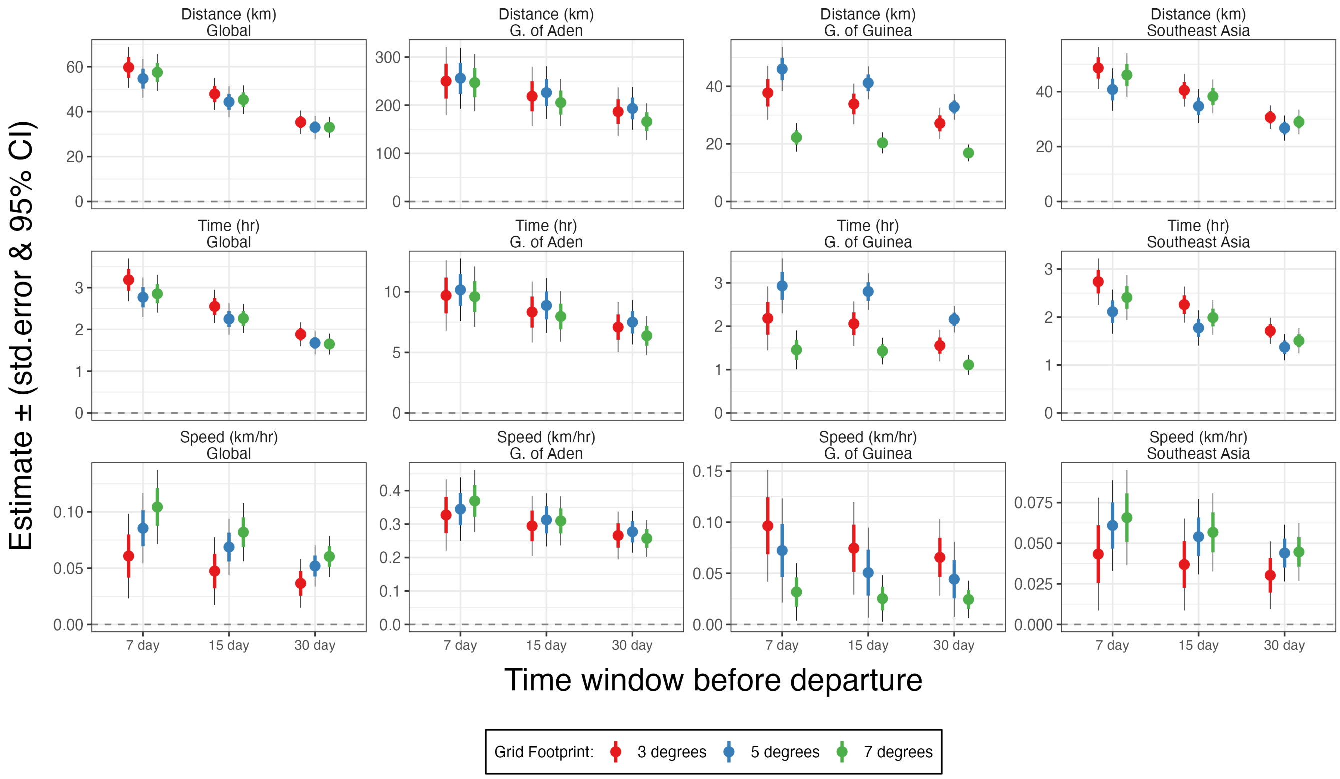

Supplementary Figure 6: **Replication Under Different Time Horizons and Degree Footprints of Vessels at Least Once Classified as Cargo.** Coefficient estimates from Equation (2) show the change in voyage features as a function of the number of pirate encounters along the voyage path in the preceding months. The sample includes vessels classified as cargo by official registries at least once. Each plot shows the results for models using time windows of 7, 15, and 30 days, respectively. Each color shows results for models using a 3, 5, and 7° spatial footprint, respectively. The thick portion of error bars shows clustered standard errors, and the thin portion shows 95% Confidence Intervals. Estimation, subsampling, specification, and clustering approach remain identical to those in Supplementary Table 1.

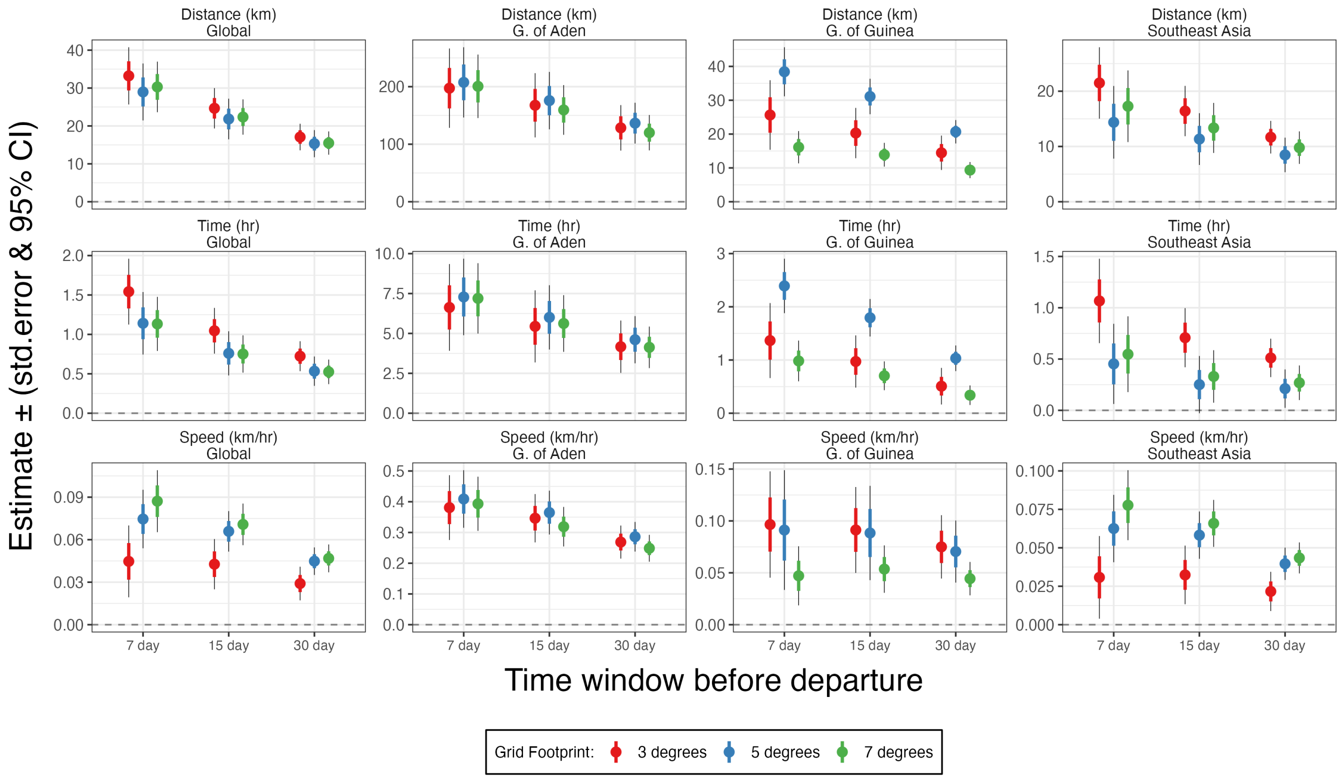

Supplementary Figure 7: **Replication Using Total Number of Encounters Under Different Time Horizons and Degree Footprints.** Coefficient estimates from Equation (2) show the change in voyage features as a function of the total number of pirate encounters along all previously traveled paths for each route in the preceding months. Each plot shows the results for models using time windows of 7, 15, and 30 days, respectively. Each color shows results for models using a 3, 5, and 7° spatial footprint, respectively. The thick portion of error bars shows clustered standard errors, and the thin portion shows 95% Confidence Intervals. Other than the explanatory variable, estimation, subsampling, specification, and clustering approach remain identical to those in Supplementary Table 1.

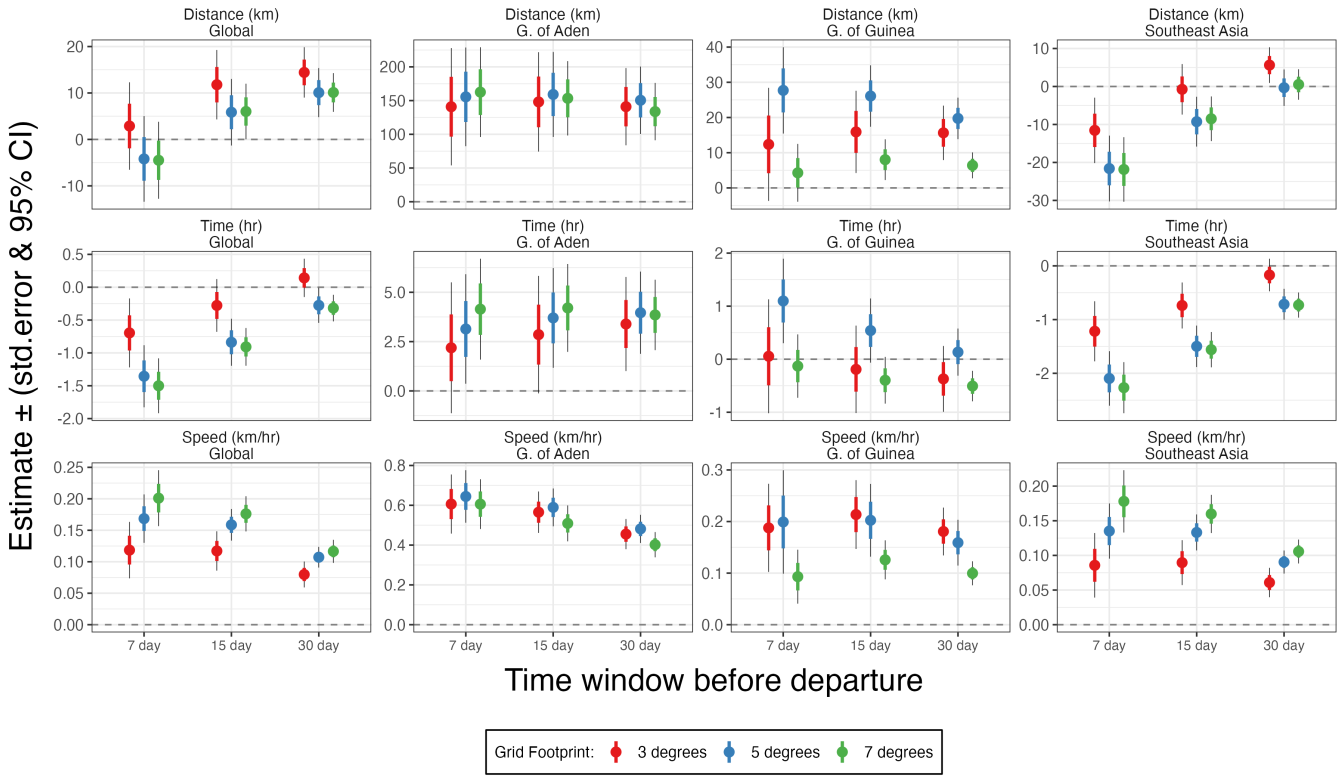

Supplementary Figure 8: **Replication Using Average Number of Encounters Under Different Time Horizons and Degree Footprints.** Coefficient estimates from Equation (2) show the change in voyage features as a function of the average number of pirate encounters along all previously traveled paths for each route in the preceding months. Each plot shows the results for models using time windows of 7, 15, and 30 days, respectively. Each color shows results for models using a 3, 5, and 7° spatial footprint, respectively. The thick portion of error bars shows clustered standard errors, and the thin portion shows 95% Confidence Intervals. Other than the explanatory variable, estimation, subsampling, specification, and clustering approach remain identical to those in Supplementary Table 1.

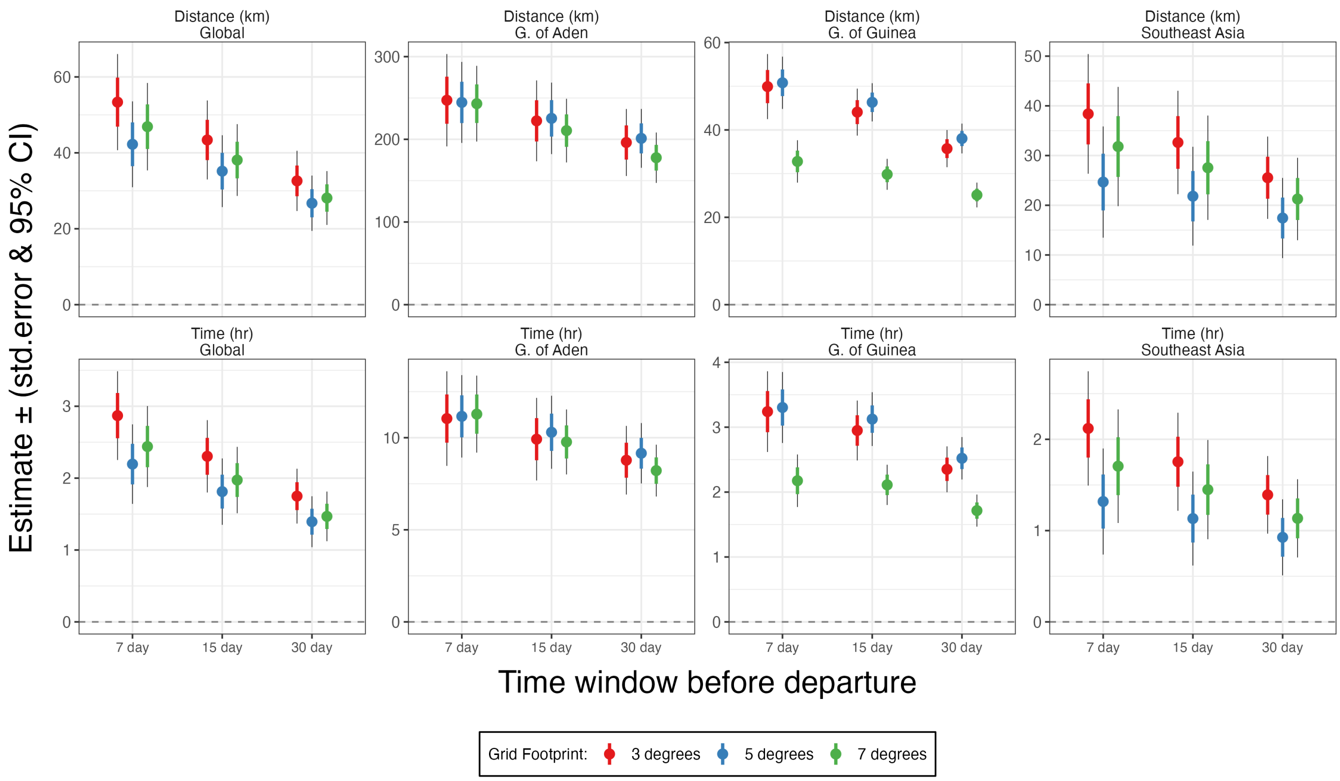

Supplementary Figure 9: **Replication Using Speed and Days Since Last Encounter as Covariates Under Different Time Horizons and Degree Footprints.** Coefficient estimates from Equation (2) show the change in voyage features as a function of the number of pirate encounters along the voyage path in the preceding months, with average speed and days since the last encounter included as additional covariates. Each plot shows the results for models using time windows of 7, 15, and 30 days, respectively. Each color shows results for models using a 3, 5, and 7° spatial footprint, respectively. The thick portion of error bars shows clustered standard errors, and the thin portion shows 95% Confidence Intervals. Other than the explanatory variables, estimation, subsampling, specification, and clustering approach remain identical to those in Supplementary Table 1.